

Two-dimensional distribution of living benthic foraminifera in anoxic sediment layers of an estuarine mudflat (Loire Estuary, France)

A. Thibault de Chanvalon^{1,2}, E. Metzger¹, A. Mouret¹, F. Cesbron¹, J. Knoery², E. Rozuel², P. Launeau¹, M. P. Nardelli¹, F.J. Jorissen¹, E. Geslin¹

[1]{Université d'Angers, Université de Nantes, LPG-BIAF, UMR CNRS 6112, 49045 Angers Cedex, France }

[2]{Ifremer, LBCM, Rue de l'Île d'Yeu, 44300 Nantes, France }

Correspondence to: A. Thibault de Chanvalon (athibaultdc@gmail.com, aubin.thibault-de-chanvalon@univ-nantes.fr)

Abstract

We present a new rapid and accurate protocol to simultaneously sample benthic living foraminifera in two dimensions in a centimetre scale vertical grid and dissolved iron and phosphorus in two dimensions at high resolution (200µm). Such an approach appears crucial for the study of foraminiferal ecology in highly dynamic and heterogeneous sedimentary systems, where dissolved iron shows a strong variability at a centimetre scale. On the studied intertidal mudflat of the Loire estuary, foraminiferal faunas are dominated by *Ammonia tepida*, which accounts for 92% of the living (CTG-labeled) assemblage. The vertical distribution shows a maximum density in the oxygenated 0-0.4 cm surface layer. A sharp decrease is observed in the next two centimetres, followed by a second well defined maximum in the suboxic sediment layer (3 - 8 cm depth). The presented method yields new information concerning the 2D distribution of living *A. tepida* in suboxic layers. First, the identification of recent burrows by visual observation of the sediment cross-section, and the burrowing activity as deduced from the dissolved iron spatial distribution show no direct relation with the distribution of *A. tepida* at a centimetre scale. This lack of relation appears contradictory to previous studies (Aller and Aller, 1986; Berkeley et al., 2007). Next, the heterogeneity of *A. tepida* in the 3-8 cm depth layer has been quantified by the Moran's Index to identify the scale of parameters controlling the *A. tepida* distribution. The results reveal horizontal patches with a characteristic length of 1 to 2 cm. These patches correspond to areas enriched in dissolved iron likely generated by anaerobic degradation of labile organic matter.

34 These results suggest that the routinely application of our new sampling strategy could yield
35 important new insights about foraminiferal life strategies, improving our understanding of the
36 role of these organisms in coastal marine ecosystems..

37

38 **1 Introduction**

39

40 Intertidal estuarine mudflats are transitional areas between land and sea. This intermediate
41 position explains the important horizontal, vertical (in the sediment column) and temporal
42 heterogeneities in physical and chemical sediment properties. It also causes heterogeneous
43 ecological niches with scales ranging from micro- to hectometres. When studying such
44 heterogeneous environments, the observational scale has to be chosen in function of the scale
45 of the studied ecological niche variability (Wu et al., 2000; Morse et al., 2003; Martiny et al.,
46 2006; Wu and Li, 2006). This is a fundamental prerequisite to further identify potential
47 parameters controlling the heterogeneity of the niches.

48

49 Ecological studies of benthic foraminifera attempt to describe the main factors controlling
50 foraminiferal communities, and their variability on different spatial and temporal scales
51 (Buzas et al., 2015). The best described pattern concerns the spatial variability of their vertical
52 distribution in open marine environments, on a hundred-kilometre scale. The conceptual
53 model proposed by (Jorissen et al., 1995) considers a regional variability of the spatial
54 organization of foraminiferal taxa in the sediment column, where they occur in a succession
55 of so-called microhabitats. The stratified succession of inhabited sediment layers is supposed
56 to be a response to oxygen and organic matter availability, which change vertically in the
57 uppermost sediment, but also geographically, when going from oligotrophic (deep water,
58 offshore) to eutrophic (shallow water, nearshore) conditions. In estuarine areas, on smaller
59 scales, other major controls are invoked (e.g. emersion time, grain size, salinity), but they are
60 less well documented. At a kilometre scale, the salinity, salinity variations and more generally
61 the frequency of chemical exchanges with the ocean are often invoked as controls of
62 foraminiferal assemblages (Debenay and Guillou, 2002; Debenay et al., 2006). Within the
63 estuary, especially in cross-shore transects, emersion time seems to be a major controlling
64 factor of species distribution at a decametre scale (Berkeley et al., 2007). But others
65 parameters, such as grain size, pH or organic carbon lability could also have a significant
66 impact. Estuarine foraminiferal faunas seem to show substantial patchiness at metre scale at

67 the sediment surface (Buzas, 1970; Hohenegger et al., 1989; Buzas et al., 2002, 2015). At a
68 decimetre scale, the rare studies performed on intertidal mudflats highlight that grain size and
69 topography could be important controls (Lynts, 1966; Morvan et al., 2006).

70

71 Finally, according to our knowledge, only three publications have analyzed the spatial surface
72 organization at a centimetre scale, using an adequate sampling grid (Buzas, 1968 in Rehoboth
73 Bay, Delaware; Olsson and Eriksson, 1974, on the Swedish coast; and de Nooijer, 2007 in the
74 Wadden Sea). These three studies show that foraminiferal densities present a patchy
75 distribution. Buzas (1968) hypothesized that this could be due to individual reproduction,
76 leading to very localized and intermittent density maxima, so called “pulsating patches”
77 (Buzas et al., 2015). Another field approach, at a centimetre scale, is to sample around
78 inhabited burrows, using a non-regular sampling scale, by defining position, size and shape of
79 each sample according to the burrow geometry. In this way (Aller and Aller, 1986; Thomsen
80 and Altenbach, 1993) studied the foraminiferal distribution around macrofaunal burrows at
81 subtidal stations and observed a threefold enrichment of foraminiferal density in the burrow
82 walls. With a similar sampling strategy, (Koller et al., 2006) showed a three hundred-fold
83 enrichment of foraminiferal densities in the burrow walls of an intertidal station. These
84 studies highlight the importance of macrofaunal activity at the centimetre scale as a potential
85 control of foraminiferal spatial organization. They suggest the presence of oxic
86 microenvironments around the burrows generated by bio-irrigation, attractive because of
87 organic matter enrichment (Aller and Aller, 1986). Foraminifera could specifically colonize
88 these environments favourable for aerobic respiration and therefore be found at depths below
89 oxygen penetration.

90

91 However, another possible explanation for the presence of rich foraminiferal faunas in deeper
92 anoxic layers could be the ability of some species to switch to alternative (*e.g.* anaerobic)
93 metabolisms (Leutenegger and Hansen, 1979; Bernhard and Alve, 1996; Risgaard-Petersen et
94 al., 2006; Heinz and Geslin, 2012). These two possible mechanisms lead to contrasted
95 conclusions concerning ecological strategies. For example, a high density of living
96 foraminifera along burrow walls compared to anoxic surrounding sediments may be explained
97 by a positive response of the foraminiferal community to the availability of oxygen and labile
98 organic matter (Aller and Aller, 1986; Loubere et al., 2011) or as the involuntary consequence
99 of passive downward transport due to macrofaunal bioturbation followed by the development
100 of a short term survival strategy based on a metabolism modification (Douglas, 1981; Alve

101 and Bernhard, 1995; Moodley et al., 1998). *In situ* distribution can answer this question by
102 determining whether subsurface high density is only concomitant with burrows or whether
103 living *A. tepida* are able to modify their metabolism in order to survive in suboxic
104 environment (without both oxygen and sulphide) independently of burrows. Unfortunately,
105 the sampling strategies used in the above mentioned references did not allow establishing the
106 importance of burrows compared to other environmental physico-chemical parameters
107 because the increased density observed in burrow walls was not compared to a “background
108 heterogeneity” at the same scale. This precaution is necessary, especially when the increase of
109 foraminiferal density is not at least one order of magnitude. Consequently, a large uncertainty
110 remains about the ubiquity and the nature of macrofauna-independent mechanisms that could
111 cause foraminiferal heterogeneity.

112

113 The recent development of pore water sampling techniques with high resolution in two
114 dimensions offers the advantage of providing simultaneously geochemical information on
115 vertical and horizontal sub-millimetre scales (Stockdale et al., 2009; Santner et al., 2015).
116 Several studies have evidenced important spatial variability of dissolved iron release into pore
117 water (Jézéquel et al., 2007; Robertson et al., 2008; Zhu and Aller, 2012; Cesbron et al.,
118 2014). This can be due to iron oxide consumption caused by local labile organic matter
119 patches that favour anaerobic respiration (by dissimilatory bacteria; Lovley, 1991) or by
120 enhancement of sulphide transport from the deeper layers through burrows and subsequent
121 abiotic dissolution (Berner, 1970). Conversely, macrofaunal water renewal is also likely to
122 bring oxic water into the burrows which consumes reduced dissolved iron and replenishes the
123 stock of iron oxide. Direct burial of iron oxide by macrofauna may also contribute to the
124 replenishment (Burdige, 2011). The overall role of macrofaunal activity on the sedimentary
125 iron cycle is still unclear (Thibault de Chanvalon et al., in prep; Robertson et al., 2009).
126 Phosphorus is also likely to have a heterogeneous geochemical pattern. Very marked
127 centimetre scale patches were reported (Cesbron et al., 2014), apparently due to nutrient
128 recycling from organic matter. However, iron oxide dissolution can also release adsorbed
129 phosphorus according to a ratio up to P/Fe ~0.2 (based on ascorbate extractions; Anschutz et
130 al., 1998) which can be compared to the theoretical anaerobic respiration ratio of P/Fe ~0.002
131 (Froelich et al., 1979). Using geochemical fingerprints, the combination of sub-millimetre
132 resolution analyses of dissolved iron and phosphorus is thus likely to (1) confirm the burrow
133 activity (iron oxidation) and (2) identify potential hotspots of organic matter consumption
134 (phosphorus production independent to iron).

135

136 In the present paper, we present a new two dimensional sampling technique allowing first the
137 investigation of the relation between benthic foraminifera and dissolved iron, and next, to
138 analyze the heterogeneity of the foraminiferal distribution and to identify the scale of potential
139 controls such as active burrows or labile organic matter patches.

140

141

142 **2 Material and methods**

143 **2.1 Site description**

144

145 The Loire estuary (NW coast of France) is hyper-synchronous: it shows an increasing tidal
146 range upstream (Le Floch, 1961) reaching a maximum spring tidal range of about 7m at 40
147 km from the mouth. At Donges (in the high tidal range area, right shore) the daily surface
148 salinity range is about 20. Seasonally, surface salinity fluctuates from 0 during floods to 30
149 during low-water periods (network SYVEL, GIP Loire Estuaire). On the opposite shore, the
150 largest mudflat of the estuary (“Les Brillantes”, ~1350 ha) extends downstream from the city
151 of Paimboeuf. During high tide, hydrodynamics (tide, wind induced waves, flow) constrains
152 the sediment deposition/resuspension cycle whereas during low tide, biological factors
153 (bioturbation, biofilm stabilization, benthic primary production; (Round, 1964; Vader, 1964;
154 Paterson, 1989) become more important and generate sediment burial and chemical
155 transformations. Microphytobenthic biofilms vary annually between 20 mg m⁻² in January and
156 60 mg m⁻² in July (Benyoucef et al., 2014). Our sampling site (47°16'56.00"N 2° 3'47.00"W)
157 is located on the slikke of “Les Brillantes” mudflat, below the Mean High Water Neap Tide
158 level (MHWNT), about 20 m offshore from an active one metre high eroded cliff. Sediment is
159 mainly composed of silt (92%) with some clay (6%) and sand (2%) (Benyoucef, 2014).

160

161 We sampled in May 2013, two weeks after a major flood (discharge volume at Paimboeuf
162 >2500 m³.s⁻¹, hydro.eaufrance.fr). During sampling the river discharge was 835 m³ s⁻¹ on
163 average. Air temperature was 12.7°C, the weather was cloudy and salinity in the surface
164 waters of the main channel ranged from 0.6 to 20 (data from SYVEL network). Sediment
165 samples were collected at the beginning of low tide. Porosity decreased from 0.917 to 0.825
166 in the first 5 cm (Thibault de Chanvalon et al., in prep). The calcite saturation state, calculated
167 from alkalinity, sodium, calcium concentrations and pH (Millero, 1979, 1995; Mucci, 1983;

168 Boudreau, 1996; Mucci et al., 2000; Hofmann et al., 2010) was above 1.0 until 9 cm depth
169 (data not shown). The macrofauna was mainly composed of *Hediste diversicolor* (Annelida:
170 Polychaeta, 630 ind m⁻²) and *Scrobicularia plana* (Mollusca: Bivalvia, 70 ind m⁻²) (I. Métais,
171 personal communication, 2015).

172

173 **2.2 1D sampling and processing**

174

175 Four cylindrical cores (diameter 8.2 cm) were sampled using Plexiglas tubes. The first two
176 cores were dedicated to foraminiferal analysis and were sliced immediately after sampling;
177 every two millimetres from 0 to 2 cm and every half centimetre between 2 and 5 cm. Surface
178 microtopography induces high uncertainty in the volume of the upper slice. Within one hour
179 after retrieval, in order to distinguish living foraminifera, sediments were incubated with the
180 staining molecule CellTracker Green™ in a final concentration of 1 μmol.L⁻¹ in 50 mL of
181 estuarine water for 10-19 hours (Bernhard et al., 2006). CellTracker Green is a non-
182 fluorescent molecule, which is hydrolyzed by nonspecific esterases, producing a fluorescent
183 compound. After incubation, samples were fixed in 3.8% Borax-buffered formalin and stored
184 until analysis. In the laboratory, samples were sieved over 315, 150, 125 and 63 μm meshes,
185 and the 150-315 μm fraction was examined using an epifluorescence stereomicroscope (i.e.,
186 485-nm excitation, 520-nm emission; Olympus ZX12 with a fluorescent light source Olympus
187 URFLT or Nikon SMZ 1500 with a PRIOR Lumen 200). All foraminifera that fluoresced
188 continuously and brightly were wet picked, air dried, identified and counted.

189

190 The two other cores were used to constrain geochemistry. The first core was dedicated to
191 microelectrode profiling and solid phase geochemistry. The solid phase was characterized by
192 total organic carbon and reactive iron, manganese and phosphorus, extracted by an ascorbate
193 reagent (buffered at pH 8) during 24 hours (Kostka and Luther III, 1995; Anschutz et al.,
194 1998, 2005; Hyacinthe et al., 2001; Hyacinthe and Van Cappellen, 2004). See more details in
195 Supplement (S1). Oxygen was analyzed with Clark's type electrodes (50μm tip diameter,
196 Unisense©, Denmark) within the first 5 mm at a 100 μm vertical resolution. In the second
197 core, Diffusive Equilibrium in Thin film in one dimension probes (DET 1D, adapted from
198 Davison and Zhang, 1994; Krom et al., 1994) were incubated during one night for dissolved
199 sodium, iron, manganese and phosphorus. Gel samples were eluted in HNO₃ 0.01 M and

200 analyzed by ICP-AES. Salinity was estimated from sodium concentration. See more details in
201 Supplement (S2).

202

203 **2.3 2D sampling and processing**

204

205 For the two-dimensional sampling, we used a “jaw device”, composed of two main parts
206 (jaws; Fig. 1). The first jaw is a DET gel probe, which samples the dissolved chemical species
207 from the pore water at high resolution, whereas the second jaw samples a 2 cm-thick slice of
208 the adjacent sediment, from which we sub-sampled 1 cm³ aliquots for foraminiferal analysis.
209 The first jaw is a 250 mm x 200 mm x 2 mm polycarbonate (Poly-methyl methacrylate) plate
210 with a central depression of 1 mm that holds a 2D gel probe. The probe is made of two layers:
211 1) a 180 mm x 97 mm x 0.92 mm polyacrylamide thin-film prepared and rinsed with Milli-Q
212 (Krom et al., 1994) which reaches equilibrium in a few hours once incubated (called “2D
213 DET gel”) and 2) a PVDF porous (0.2 µm) membrane to protect the gel, prevent falling out
214 the depression and control diffusion. The 2D DET gel was prepared and mounted less than
215 one week before sampling, conserved in a wet clean plastic bag and was deaerated by N₂
216 bubbling for about 6h before deployment. The sampler was deployed into the sediment at low
217 tide. On both lateral sides of the central depression (Fig. 1), plastic rails (2 cm high) were
218 fixed in order to guide the second jaw to slide along the plate. The second jaw is a stainless
219 steel plate (1.5 mm thick) bent on both sides. After equilibration (5h) of the 2D gel, the
220 second jaw was inserted along the guides of the first jaw and the whole device was gently
221 pulled out of the sediment. Once on shore the 2D gel was separated from the sediment,
222 covered with a plastic-coated aluminium plate and stored in an icebox with dry ice pellets
223 (Cesbron et al., 2014), until final storage in a freezer (-18°C).

224

225 The sediment plate was manually cut (with stainless steel trowels) within 30 minutes in 1 cm³
226 cubes for a surface of 8 cm x 8 cm. The resulting sampling map is presented in Fig. 2 together
227 with the 1D sampling scheme of foraminifera. Next, these sediment cubes were labelled with
228 CTG to recognize living foraminifera (as for the core slices, see 2.2). Considering an error of
229 1 mm for each cut, the volume uncertainty was ~14%, except for surface samples where the
230 microtopography of the sediment surface considerably increases volume uncertainty.

231

232 The 2D DET probe was analyzed in order to obtain the concentrations of dissolved iron and
233 dissolved reactive phosphate (DRP) (Cesbron et al., 2014). Quickly, after thawing at ambient
234 temperature, the sample gel was recovered by a reactive gel equilibrated in specific
235 colorimetric reagents. Twenty five minutes after contact, a picture (reflectance analysis) of
236 superposed gels was taken with a hyperspectral camera (HySpex VNIR 1600) and analyzed
237 (see 6.3 for more details). The resolution (surface area of pixels) was 211 μm x 216 μm . The
238 estimated incertitude is 10% for iron and 11% for DRP. See more details in Supplement (S3).
239 To compare the geochemical species distribution (at submillimetre resolution) and
240 foraminiferal density (at centimetre resolution), a handmade R code was written allowing the
241 downscaling of chemical resolution from 0.2 mm to 1 cm.

242

243 **2.4 Statistical analyses**

244

245 Patchiness effect or autocorrelation, interpreted as the fact that the density of one square
246 depends on its neighbours, was explored using spatial correlograms built using Moran's Index
247 (I), computed with R (package "spdep" following (Fortin and Dale, 2005; Bivand et al., 2008;
248 Legendre and Fortin, 2010; Borcard et al., 2011), equation (1)). This index was applied to
249 benthic meiofauna by (Blanchard, 1990) and (Eckman and Thistle, 1988) and to foraminifera
250 by (Hohenegger et al., 1993). This index calculates the similarity of pair values for one
251 neighbourhood, a neighbourhood being defined by a weight ($w_{i,j}$) function of the distance (d)
252 between pairs.

$$253 \quad I(d) = \frac{\sum_{i,j}^n w_{i,j}(d)(x_i - \bar{x})(x_j - \bar{x})}{\sqrt{\sum_i^n (x_i - \bar{x})^2}} \times \frac{n}{\sum_{i,j}^n w_{i,j}(d)} \quad (1)$$

254 Here, the 40 cubes used for Moran's Index have neighbourhood defined as cubes in direct
255 contact (4 neighbours per sample with a weight of 1, others have 0, also known as "rook
256 connectivity" (Fortin and Dale, 2005)). With this configuration, Moran's Index is -1 for a
257 contrasted organization (perfect negative correlation between neighbours) and +1 in case of
258 grouped organization (perfect positive correlation between neighbours). A value of I=0
259 corresponds to no organization or random distribution. The correlogram plots Moran's Index
260 versus the order of the neighbours (o.n.). A decrease of the Moran's Index from positive to
261 negative values characterizes a patchy distribution. The characteristic length of the patchiness
262 is defined as the order of neighbours when $I_{o,n.}=0$ (Legendre and Fortin, 1989). Two
263 dimensional non-random organization has been tested with the alternative hypothesis $I_{o,n.}>I_0$

264 where I_0 is determined with a Monte-Carlo method. The second test examines if there is a
265 preferential direction in the organization (isotropy). Again, the alternative hypothesis $I_{0,n} > I_0$
266 for Moran's Index is used, restricting the distance to the tested dimension (vertical or
267 horizontal). Thus, in our case, each sample was compared only with its lateral or vertical
268 neighbours (i.e., 2 neighbours per test).

269 **3 Results**

270 **3.1 1D geochemical features**

271

272 Figure 3 shows both solid and dissolved chemical species obtained from the dedicated cores.
273 Total organic carbon (C_{org} , black circles, Fig. 3A) decreased from $2700 \mu\text{mol g(dry sed)}^{-1}$ to
274 $1900 \mu\text{mol g(dry sed)}^{-1}$ in the first centimetre, then increased sharply until 1.5 cm depth, and
275 finally decreased progressively from $2700 \mu\text{mol g(dry sed)}^{-1}$ to $2400 \mu\text{mol g(dry sed)}^{-1}$ at 5
276 cm depth. Salinity (Fig. 3A) ranges from 7.5 to 1.7 with an offset of ~ 2 between replicates
277 and a decrease of ~ 3 in the 13 first centimetres. Figure 3B shows the vertical distribution of
278 dissolved oxygen. The three profiles shown (out of 18) are considered representative of the
279 lateral variability in the sediment. Most of the oxygen concentration profiles show the
280 exponential trend typical for undisturbed marine sediments (2 profiles in Fig. 3B, with light
281 grey and white diamonds; (Revsbech et al., 1980; Berg et al., 1998). However, one third of
282 the O_2 profiles diverged from the exponential model, showing an interruption of the
283 decreasing trend, or even a local increase, at depth (e.g. the profile with dark grey diamonds
284 represented in Fig. 3B). The Oxygen Penetration Depth (OPD) remained relatively constant
285 around 2.0 mm (sd=0.2 mm, n=18) despite this heterogeneity.

286

287 Figures 3C, 3D and 3E show the distribution of manganese, iron and phosphorus,
288 respectively, both in the dissolved phase (grey and open diamonds) and in the easily reducible
289 solid phases (black circles, extracted by ascorbate leaching (Anschutz et al., 2005; Hyacinthe
290 et al., 2006)). Extracted manganese (mainly (hydr)oxide, black circles in Fig. 3C) showed a
291 strong enrichment of the easily reducible solid phase (until $13 \mu\text{mol g(dry sed)}^{-1}$) in the first
292 two millimetres, where an important upward diminution was visible in both replicates of the
293 dissolved phase (grey and open diamonds in Fig. 3C). Below, the solid phase showed a
294 slightly decrease from 7.9 to $5.6 \mu\text{mol g(dry sed)}^{-1}$ until 5 cm depth. The dissolved manganese
295 concentration decreased between 4 and 9 cm depth in both replicates (from 70 to $30 \mu\text{mol L}^{-1}$).
296 In the solid phase, iron, phosphorus and manganese are strongly correlated when the

297 surface sample is not considered ($r^2=0.70$ and 0.55 between iron and manganese, and iron and
298 phosphorus, respectively). Profiles of dissolved iron and phosphorus are also strongly
299 correlated ($r^2=0.90$, slope= 1.87 and $r^2=0.47$, slope= 1.31 for replicates A and B). Iron and
300 phosphorus were remobilized, and therefore appeared in the dissolved phase, between 1 and 9
301 cm. Both replicates of dissolved iron showed the same four well described maxima (at least
302 six samples for each maximum) at 2.3, 3.3, 5.9 and 7.3 cm depth but with different
303 concentrations. In replicate A (open diamonds) these maxima have five times higher iron
304 concentrations (up to $700 \mu\text{mol L}^{-1}$) than in replicate B.

305

306 **3.2 Visual features on the sediment plate**

307

308 Figure 4A shows the sediment slice obtained from the “jaw device” facing the 2D DET gel. In
309 order to facilitate the description, the figures were subdivided in centimetre squares labelled
310 with letters for the horizontal position and numbers for the vertical position. The black
311 rectangle corresponds to the 2D DET gel position, the blue rectangle to the gel signal
312 exploited and the red rectangle to the 2D foraminiferal sampling. Burrows parallel to the
313 cutting plan are visible over their entire length. When perpendicular to the cutting plan, they
314 appear as a dark hole (B14 in Fig. 4A). Figure 4B summarizes burrow distributions
315 superimposed on a picture of the gel after equilibration with the colorimetric reagents (pink
316 coloration corresponds to iron and blue to dissolved reactive phosphorus (DRP)). Five
317 burrows were visibly connected to the sediment surface; their traces mostly extended
318 vertically down to 10 cm depth where their track is lost. Between 10 and 15 cm depth, visible
319 burrow density decreased. Below 15 cm depth, burrows were rarely observed and the
320 sediment was dark (Fig. 4A). During slicing of the sediment plate, living polychaetes (*Hediste*
321 *diversicolor*) were observed in some burrows.

322

323 **3.3 2D DET gel**

324

325 Figure 5 shows the 2-dimensional datasets, with the distribution of dissolved phosphorus (Fig.
326 5A) and iron (Fig.5B) obtained from the 2D DET gel. For comparison, burrow distribution is
327 shown in Fig. 5A. Dissolved iron and phosphorus both appeared a few millimetres below the
328 sediment-water interface. They are positively correlated for the whole plate ($r^2= 0.59$,
329 slope= 2.7). Despite their patchy distribution, both species can be observed along the entire

330 length of the gel probe (i.e. 17 cm depth). A main feature was the occurrence of two
331 prominent vertical structures enriched in dissolved iron and in DRP (A-B/6-9 and F-G/5-14).
332 The highest concentrations, of about 170 and 50 $\mu\text{mol L}^{-1}$ for iron and phosphorus,
333 respectively, were found within the structure at the right (squares F/8-9). In the structure at the
334 left (A/6-8), iron and phosphorus maxima were around 120 and 25 $\mu\text{mol L}^{-1}$, respectively.

335

336 Most burrows seem to impact the iron concentration. For example, burrows 1, 3 and 5 clearly
337 correspond (in the 4 first centimetres) to a drastic decrease or even disappearance of dissolved
338 iron, whereas other burrows seem to correspond to a dissolved iron enrichment (F-G/5-9).
339 However, some cm size patches (e.g. A-B/6-9, H-G/8-9 and F-G/17) seem to be unrelated to
340 burrow structures. Below 15 cm depth, the sediment was dark and dissolved iron generally
341 decreased whereas DRP increased.

342

343 **3.4 Living foraminiferal distribution**

344

345 Figure 5C shows the distribution of CTG-labelled *Ammonia tepida* determined for 1cm^3
346 samples in the sediment facing the 2D DET gel. The analysis of living foraminifera in the 64
347 cubes (8 cm width * 8 cm depth) takes roughly the same time as the analysis of one core of
348 8.2 cm of diameter (until 5 cm depth). *Ammonia tepida* was by far the dominant species,
349 accounting for 92% of the total assemblage. The second most frequent species, *Haynesina*
350 *germanica*, represented 5% but its low density (mostly 0, 1 or 2 individuals per cubic
351 centimetre) was not sufficient to support a reliable discussion. For this reason the data relative
352 to this species are omitted from the present paper. *A. tepida* density ranged from 0 to 38 ind
353 cm^{-3} with important lateral and vertical variability. The relative standard deviation (rsd)
354 calculated for each row is, on average, 45%, whereas for each column the rsd is 60%,
355 suggesting a slightly more pronounced vertical organization. This is confirmed by the
356 stratification of the richest samples (≥ 27 ind cm^{-3}) which were found in the topmost cm and
357 below 6 cm depth, whereas the poorest samples (≤ 5 ind cm^{-3}) were found between 1 and 3
358 cm depth. Each row from the 2D distribution can be represented by a whisker plot (Fig. 6).
359 The results confirm a three-step pattern with high densities at the surface (13 to 38 ind. cm^{-3}),
360 lower density between 1 and 3 cm depth (0 to 12 ind cm^{-3} and one outlier at 24 ind. cm^{-3}) and
361 increasing values below 3 cm (7 to 31 ind cm^{-3}).

362

363 This vertical pattern is also visible in the two studied sediment cores (Fig. 6): high densities of
364 *A. tepida* (26 ± 0 ind. cm^{-3}) are observed in the first 2 mm, a rapid decrease to minimal
365 densities in the 1.0 - 1.2 cm layer (3 ± 0 ind. cm^{-3}), followed by a progressive, somewhat
366 irregular increase until 9 ± 0 ind. cm^{-3} below 2 cm depth to 8cm depth. Despite the different
367 vertical sampling resolution, the densities observed in the cores are in agreement with the
368 average densities observed in the sediment slice cubic samples.

369

370

371 4 Discussion

372 4.1 A methodological improvement to characterize heterogeneity

373

374 Here, we present for the first time a methodology allowing to study simultaneously the
375 vertical and horizontal heterogeneity of chemical species and living foraminifera (determined
376 by CTG labelled) in the 8 first centimetres of the sediment. Figure 6 compares the vertical
377 density distribution of *A. tepida* between the cores (triangles) and the jaw device (whisker
378 plots), sampled a few decimetres apart. Despite the different vertical sampling resolution, the
379 densities observed in the cores (sampling surface of 53 cm²) are in agreement with the
380 average densities observed in the sediment slice samples (sampled with the “jaw device”,
381 sampling surface of 8 cm²). This similarity suggests a limited horizontal heterogeneity of *A.*
382 *tepida* at a decimetre scale, although it is impossible to draw firm conclusions on the basis of
383 only three samples (the two cores and the jaw device).

384

385 The jaw device (boxplot whiskers, Fig. 6) reveals a heterogeneous horizontal distribution at
386 the centimetre scale. The centimetre heterogeneity is quantified by calculating the Moran's
387 Index that estimates the characteristic length of foraminiferal niches. Figure 7 shows the
388 Moran's Index correlograms applied between 3 and 8 cm depth where high densities of living
389 foraminifera are observed in suboxic sediments. Figure 7A shows that the spatial organization
390 of *A. tepida* is patchy at a centimetre scale ($I_1=0.24$, p-value=0.013). For farther neighbours
391 the Moran's Index values drop to zero, describing a random organization. Concerning vertical
392 and horizontal heterogeneities, Moran's index values for direct neighbours are 0.02 and 0.47,
393 with p-values of 0.38 and 0.001, respectively. For second order neighbours, values do not
394 significantly differ from 0 in either direction (data not shown). This means that *A. tepida*
395 specimens tend to be grouped in horizontal spots with a characteristic length of 1 to 2 cm.

396

397 Figure 7B shows the Moran's Index correlogram for iron at 1cm scale resolution (phosphorus
398 is similar and not shown). It shows strong patchiness ($I_1=0.7$) for direct neighbours in either
399 direction, with a characteristic length of 3-4 cm. The fact that the characteristic lengths of *A.*
400 *tepida* (Fig. 7A) and dissolved iron (Fig. 7B) patches are longer than 1 cm suggests that the
401 impact of different sampling thicknesses (roughly null for dissolved iron against 1 cm for
402 foraminifera) would not result in major bias. Moreover, this characteristic length is important
403 as it likely corresponds to the characteristic length of the controlling mechanisms (Clark,

404 1985; Wu and Li, 2006). In fact, the difference in Moran's Index between chemical species
405 and the *A. tepida* density distribution suggests that not exactly the same mechanisms control
406 these parameters. This is an unexpected result, since most conceptual models explain benthic
407 foraminiferal distribution in the sediment as a direct response to geochemical gradients,
408 especially oxygen and sulphide (Jorissen et al., 1998; Van der Zwaan et al., 1999; Fontanier et
409 al., 2002; Langezaal et al., 2006; Langlet et al., 2013), and dissolved iron is intimately
410 coupled with these chemical species.

411

412 **4.2 Factors generating chemical heterogeneity**

413

414 The heterogeneity of geochemical patterns is mainly explained by the availability of oxidants
415 mineralizing organic carbon. In the generally applied conceptual model of Froelich et al.,
416 (1979), organic matter remineralization is characterized by a succession of horizontal layers
417 characterised by different oxidants. Figure 3 confirms this theoretical vertical stratification:
418 oxygen is rapidly consumed by respiration (about 2 mm depth, Fig. 3B); next, reduced
419 dissolved manganese appears (Fig. 3C). Dissolved iron appears still deeper, with a first
420 maximum at 2 cm depth. The slopes of the concentration profiles are steeper and the reactive
421 solid phase (Figs. 3D and 3C) is more concentrated for iron than for manganese, suggesting a
422 higher reactivity. However, the strictly vertical succession of redox layers is no longer
423 respected in the deeper suboxic layers, as shown by the multiple maxima of iron in figure 3D
424 and the high lateral heterogeneity observed in Figs. 5A and 5C. This high lateral
425 heterogeneity cannot be explained by vertical diffusion of oxygen. It appears therefore that a
426 strictly vertical stratification of redox zones, defining a similar foraminiferal microhabitat
427 succession, is not a reasonable assumption, in our study area.

428

429 **4.2.1 Macrofaunal impact on heterogeneity**

430

431 Macrofauna is assumed to be the most important cause of chemical heterogeneity at a scale of
432 0.01cm (roughly the foraminiferal scale) to 100 cm (station scale), because of its ability to
433 reorganize the sediment. In this way, macrofauna determines whether other factors can impact
434 the heterogeneity of dissolved iron and/or *A. tepida*. Macrofauna modifies: i) the sediment
435 texture/composition (burrow walls or fecal pellets); ii) the redox conditions, by ventilation of
436 their burrows with oxygenated water (bioirrigation) and iii) particle arrangement, by crawling

437 or burrowing (biomixing) (Meysman et al., 2006). The efficiency of biomixing to homogenize
438 the sediment mainly depends on two aspects (see Wheatcroft et al., 1990; Meysman et al.,
439 2010a for a more detailed discussion):

440 (1) the biomixing species assemblage. At the “Les Brillantes” mudflat, the main
441 macrofaunal species are *Hediste diversicolor* (630 ind m⁻²) and *Scrobicularia plana* (70 ind
442 m⁻², I. Métais, personal communication, 2015). *H. diversicolor* is a gallery-diffusor (particle
443 mixing due to burrowing activity) whereas *S. plana* is an epifaunal biodiffusor (particles are
444 mixed in a random way over short distances along the surface (e.g., (François et al., 2002;
445 Kristensen et al., 2012)). These two species generate homogeneity or heterogeneity according
446 to the second criterion:

447 (2) the relation between the average time of existence of the studied objects (here
448 foraminifera and dissolved iron) in the bioturbated area and the average time between two
449 bioturbation events. Frequent bioturbation events generate efficient mixing (homogeneity)
450 whereas rare bioturbation events generate heterogeneity. The average time between two
451 bioturbation events is estimated days to months by tracer modeling (Wheatcroft et al., 1990;
452 Meysman et al., 2003, 2008) while the longevity of foraminifera in suboxic environments is
453 estimated to roughly one year (Langlet et al., 2013; Nardelli et al., 2014) and the mean
454 residence time of iron in the dissolved phase is estimated between 2 and 3 days (Thibault de
455 Chanvalon et al., in prep). Therefore, biomixing should generate a homogeneous distribution
456 of foraminiferal density distribution, contrasting with a heterogeneous distribution of
457 dissolved iron (and DRP). The different timespans also suggest that most of the living
458 foraminifera were already present in the suboxic sediment before the visible (most recent)
459 burrows were created. Conversely, the heterogeneity of the dissolved chemical species should
460 be directly related to biomixing and to others factors that have not been homogenised by
461 biomixing *i. e.* with a short time of existence in suboxic environments.

462

463 **4.2.2 Geochemical impact of biogenic factors**

464

465 The factors likely to generate chemical heterogeneity are : (1) Bioirrigation, that mainly
466 causes an increase of oxidant availability (Aller and Aller, 1986; Aller, 2004; Arndt et al.,
467 2013), and (2) Biogenic particles (e.g. decaying macrofauna, fecal pellets), that cause an
468 increase of labile carbon availability. Dissolved iron shows two opposite types of behavior
469 (Aller, 1982): (1) iron precipitates as a hydroxide when the oxidative state of the pore water

470 surrounding active burrows increases (Meyers et al., 1987; Zorn et al., 2006; Meysman et al.,
471 2010b). This is confirmed by visible burrows in Fig. 5 in which both dissolved iron and DRP
472 are depleted (Figs 4, numbers 1, 3, 5 (above 6cm depth) and burrows in B-C-D13, E9-11,G-
473 H10-15 and A-B9). These structures are mainly vertical and have a length often exceeding 3
474 cm; in agreement with the Moran's Index correlogram. Conversely, in the long burrow F-G/5-
475 9, dissolved iron is enriched, indicating that this burrow is abandoned, so that there is no
476 oxygen renewal. This feature was also observed for some burrows by (Zhu and Aller, 2012;
477 Cesbron et al., 2014). (2) Dissolved iron is produced by anaerobic respiration where biogenic
478 particles increase labile carbon availability, and thereby decrease the oxidative state of
479 surrounding pore waters (Robertson et al., 2009; Stockdale et al., 2010). The geometry and
480 isolation from visible burrows of patches A/7-8, G-H/8-9 and F-G17 in Figs. 5A and 5B
481 suggest that they could represent centimetre-wide labile organic matter patches. We
482 hypothesize that these patches correspond to intense remineralization of biogenic particles
483 that dissolves iron oxides.

484

485 **4.3 Mechanisms controlling the *A. tepida* distribution**

486

487 The Figs. 5C and 6 clearly describes a three-step pattern in the distribution of *A. tepida*, with
488 high densities at the surface, low densities between 1 and 3 cm depth and a somewhat
489 surprising increase below (in suboxic sediments). A similar pattern was reported, but not
490 discussed, from a few replicates from (Alve and Murray, 2001; Bouchet et al., 2009) in
491 intertidal environments. In our study, the consistence of the 8 vertical columns from the plate
492 sampling confirm the robustness of this pattern and the two dimensional approach reveals an
493 organization of *A.tepida* in centimetre-wide patches in suboxic sediments. The next
494 subchapters treat the question what mechanisms are able to explain these features, especially
495 in the suboxic environment where active burrows (supporting biomixing and bioirrigation)
496 and biogenic particles have been identified as factors likely to generate such heterogeneity. .

497

498 **4.3.1 Foraminiferal metabolism**

499

500 Generally, aerobic metabolism is considered as the dominant mechanism in oxic conditions
501 since it is energetically most efficient. In fact, Figs. 5C and 6 clearly describe maximal
502 densities of *A. tepida* at the sediment surface (0-2 mm depth) and low densities below (6-18

503 mm depth). This strong gradient of *A. tepida* density highlights the presence of a continuously
504 oxygenated microhabitat enriched in organic matter (see TOC and O₂ profiles, Fig. 3A-B)
505 close to the sediment-water interface, favourable for *A. tepida*. Energetic considerations and
506 some observations that report a strong seasonal variability in the oxic zone (Moodley, 1990;
507 Barmawidjaja et al., 1992), led (de Stigter et al., 1999; Berkeley et al., 2007) to assume that
508 foraminifera reproduce preferentially in the oxic layer. Together, these factors explain the
509 maximum density in the surface layer.

510 Since the work of (Richter, 1961), numerous publications (Jorissen et al., 1992; Moodley and
511 Hess, 1992; Bernhard and Sen Gupta, 2003) have reported living benthic foraminifera in
512 suboxic sediment layers. For intertidal environments, studies have reported living (Rose
513 Bengal stain) foraminifera in subsurface environments since the 1960's (*e. g.* Buzas, 1965,
514 Steineck and Bergstein, 1979). Several *in situ* (Goldstein et al., 1995; Bouchet et al., 2009)
515 and laboratory studies (Moodley and Hess, 1992; Moodley et al., 1998; Pucci et al., 2009;
516 Nardelli et al., 2014; Nomaki et al., 2014) with *A. tepida* also reported survival, activity and
517 even calcification in suboxic conditions. Anaerobic metabolism would be a logical
518 mechanism to explain the presence of large amounts of living foraminifera in suboxic layers.
519 Complete or partial (with endo and/or ectobionts; Bernhard and Alve, 1996) denitrification
520 co-occurring with nitrate storage has been demonstrated for some foraminiferal taxa
521 (Risgaard-Petersen et al., 2006). Nomaki et al., (2014) have suggested denitrification by
522 endobionts for *A. tepida*. However, denitrification has not been measured in *A. tepida*, and
523 only very low intracellular nitrate concentrations were found (Pina-Ochoa et al., 2010; Geslin
524 et al., 2014). It appears therefore unlikely that the abundance of living *A. tepida* in deeper
525 suboxic layers can be explained by active colonization.

526

527 **4.3.2 Burying and burrow microenvironment**

528

529 It is clear that biomixing is a likely mechanism to explain the introduction of foraminifera in
530 deeper sediment layers, by passive transport (Alve and Bernhard, 1995; Goldstein et al., 1995;
531 Moodley et al., 1998; Saffert and Thomas, 1998; Alve and Murray, 2001; Jorissen, 2003).
532 However, the spatial distribution resulting from this passive transport has never been well
533 described, or modelled. According to the theory of biomixing, we suggest that the vertical
534 distribution of *A. tepida* can be approached by a diffusion model, which should lead to an
535 exponential downward decrease, with the slope function of the dead rate. Possibly, *A. tepida*

536 is able to survive in suboxic environments using an intermittent aerobic metabolism, using the
537 oxygen that can be punctually available due to bioirrigation (Fenchel, 1996; Wang et al.,
538 2001; Wenzhofer and Glud, 2004; Pischedda et al., 2012). Their activity should progressively
539 decrease once oxygen is depleted; (Phipps, 2012) suggested that they could finally become
540 immobilized before dying in case of a prolonged absence of oxygen supply. We think that
541 repeated introductions by macrofaunal bioturbation, followed by reduced metabolic activity,
542 leading to immobilisation, is the most likely mechanism to explain the high abundances of
543 living foraminifera in suboxic sediments.

544

545 Figures 4A and 5B show no relation between visible burrows and living *A. tepida*. This result
546 is in agreement with the different time-scales of the foraminiferal lifespan and the burrows,
547 and with the idea that biomixing homogenizes the *A. tepida* density. It suggests also that the
548 oxygenation obviously generated by formation of new burrows is consumed too fast to allow
549 all infaunal *A. tepida* to migrate to these active burrows. Thus, recent burrow walls are
550 apparently not colonized by specimens of *A. tepida*, already present in the suboxic sediment.
551 Our observations contrast with earlier studies, showing increased foraminiferal densities (up
552 to 300 times higher than in the surrounding sediment, rose Bengal stained) in burrow walls.
553 For example, data from burrows of *Amphicteis* sp. at 4800m depth (Aller and Aller, 1986), of
554 *Echiurus echiurus* at 42m depth (Thomsen and Altenbach, 1993) and of *Pestarella tyrrhena*
555 in intertidal sandflats (Koller et al., 2006) all presented high foraminiferal densities. The
556 observed differences could be due to the fact that burrows of various macrofaunal taxa may
557 represent very different conditions and lifespans and eventually to a difference in sampling
558 scale, since Thomsen and Altenbach (1993) and Koller et al. (2006) applied an irregular
559 millimetre sampling around burrows. Summarizing, macrofaunal activity would explain
560 transport to and survival in suboxic layers. However, it does not explain the density minimum
561 at 1-3 cm depth.

562

563 **4.3.3 Sensitivity to geochemical gradients**

564

565 We think that the most probable explanation for the 1-3 cm density minimum of *A. tepida*, is
566 an active upward migration of the specimens, back to the sediment surface, before they are
567 completely immobilized by a lack of oxygen and a strongly lowered metabolism. Numerous
568 studies have already reported that vertical migration of foraminifera allows them to move to

569 more hospitable environments (Jorissen, 1988; Van der Zwaan and Jorissen, 1991; Alve and
570 Bernhard, 1995; Moodley et al., 1998; Gross, 2000; Langezaal et al., 2003; Geslin et al.,
571 2004; Ernst et al., 2005). In an experiment in which populations of *Haynesina germanica*
572 were uniformly mixed in a 6 cm sediment column, Ernst et al. (2006) saw a clear migration
573 back to the surface for the foraminifera living between 1 and 3 cm depth, and suggested that
574 foraminifera living at greater depth were unable to do so. Similarly, Hess et al. (2013) showed
575 that benthic foraminifera are able to migrate through suboxic sediment to reach oxic
576 sediments over a maximal distance of a few centimetres. Active migration towards directly
577 detected oxygen or organic matter over distances beyond 1 cm seems improbable, since this
578 distance is much higher than the typical pseudopodial length (about 1 cm, see Travis and
579 Rabalais, 1991). However, as described above, the presence of oxygen could be indirectly
580 detected by other geochemical gradient (e.g. NO_3^- , Mn^{2+} or Fe^{2+} , DOM (dissolved organic
581 matter), pCO_2). However, when gradients generated by the oxygen front are imperceptible for
582 *A. tepida*, because they are living too deep in the sediment, or when such gradients are hidden
583 by other sources of geochemical gradients (as organic-rich patches), this upward migration
584 could no longer occur. This could explain why below 3 cm depth, *A. tepida* remains in the
585 deeper sediment layer after being transported there accidentally.

586
587 However, the organization of the foraminiferal in 1 to 2 cm-wide horizontal patches identified
588 by Moran's Index suggests that *A. tepida* detects not only vertical geochemical gradients, but
589 probably also lateral gradients around degrading biogenic particles. The characteristic length
590 of patches of biogenic particles identified by dissolved iron (A/7-8, G-H/8-9 and F-G17 in
591 Fig. 7C and 7D, see 4.2.2) and of the foraminiferal density maxima are in agreement. For the
592 8 first centimetres, the two identified biogenic particles (A/7-8, G-H/8-9 in Fig. 5B) both
593 correspond to a higher density of *A. tepida* (28/19 and 21/30 ind cm^{-3} in average for A/7-8 and
594 G-H/8 respectively, Fig. 5C). In agreement with these results, we hypothesize that even in
595 deeper suboxic layers, where foraminifera would have a lowered metabolism most of the
596 time; they would have a limited capacity to move towards patches of labile organic matter.
597 Nevertheless, a better identification of labile carbon patches, replicate sampling with the here
598 developed strategy and experimental studies with artificial geochemical gradients are
599 necessary to confirm our hypotheses about the behaviour of *A. tepida* in suboxic
600 environments.

601

602 Summarizing, we suggest that the distribution of *A. tepida* can be interpreted as the result of
603 not less than five interacting mechanisms (Fig.8). 1) high foraminiferal densities at the surface
604 are the result of the presence of abundant labile organic matter and reproduction in the
605 oxygenated layer (§4.3.1), 2) downward transport by macrofaunal bioturbation introduces living
606 foraminifera in deeper sediment layers (§4.3.2), 3) in the 3 first centimetres foraminifera are
607 capable to migrate back to the oxygenated, organic-rich surface layers once they detect redox
608 gradients, whereas in deeper sediment layers, they are no longer capable to find their way
609 back to the superficial oxygenated layer (§4.3.3), 4) after a prolonged presence in suboxic
610 conditions, foraminifera lower their metabolism and become inactive, 5) foraminifera can
611 become temporarily re-mobilized during intermittent bioirrigation events, and can eventually
612 migrate toward organic-rich microenvironments in their vicinity (§4.3.3). A better
613 identification of labile carbon patches, for example based on alkalinity (Bennett et al., 2015),
614 pCO₂ (Zhu et al., 2006; Zhu and Aller, 2010) or dissolved organic carbon should permit to go
615 further in the interpretation.

616

617 **5 Conclusion**

618

619 We present a new, simple and robust sampling protocol, to obtain the 2D distribution of
620 benthic foraminifera combined with the 2D distribution of geochemical species. Our
621 observations on an estuarine mudflat show an important density of *A. tepida* in suboxic
622 environments with a characteristic length of patches of 1 to 2 cm. This technique was coupled
623 with a visual observation of burrow features and with analysis of dissolved iron and
624 phosphorous in 2D. These geochemical observations allowed us to recognise active burrows
625 (with minimal dissolved concentrations), and to determine that areas of dissolved iron and
626 phosphorus enrichment do not always represent abandoned burrows. Surprisingly, no direct
627 relation was found between active burrows and the *A. tepida* distribution. However, an
628 enrichment of *A. tepida* was observed in some areas with maxima of dissolved iron, suggesting
629 that even in hypoxic environments, there is a relation between the spatial distributions of *A.*
630 *tepada* and labile organic matter remineralisation. Our results show that the new sampling
631 strategy proposed here can yield important new insights in the functioning of suboxic
632 environments in estuarine mudflats.

633

634 **Acknowledgements**

635 This study is part of the RS2E – OSUNA project funded by the Région Pays de la Loire.
636 Special thanks are due to Didier Jézéquel from IPGP who designed the « jaw device ». Thanks
637 to Clement Chauvin, Cyrille Guindir, H el ene Koroshidi and Eve Chauveau for their support in
638 the field and laboratory.

639

640 **References**

641 Aller, J. Y. and Aller, R. C.: Evidence for localized enhancement of biological associated with
642 tube and burrow structures in deep-sea sediments at the HEEBLE site, western North Atlantic,
643 Deep Sea Res. Part Oceanogr. Res. Pap., 33(6), 755–790, doi:10.1016/0198-0149(86)90088-
644 9, 1986.

645 Aller, R. C.: The Effects of Macrobenthos on Chemical Properties of Marine Sediment and
646 Overlying Water, in *Animal-Sediment Relations*, edited by P. L. McCall and M. J. S. Tevesz,
647 pp. 53–102, Springer US. [online] Available from:
648 http://link.springer.com/chapter/10.1007/978-1-4757-1317-6_2 (Accessed 22 August 2014),
649 1982.

650 Aller, R. C.: Conceptual models of early diagenetic processes: The muddy seafloor as an
651 unsteady, batch reactor, *J. Mar. Res.*, 62(6), 815–835, doi:10.1357/0022240042880837, 2004.

652 Alve, E. and Bernhard, J. M.: Vertical migratory response of benthic foraminifera to
653 controlled oxygen concentrations in an experimental mesocosm, *Oceanogr. Lit. Rev.*, 42(9),
654 137–151, doi:<http://dx.doi.org/10.3354/meps116137>, 1995.

655 Alve, E. and Murray, J. W.: Temporal Variability in Vertical Distributions of Live (stained)
656 Intertidal Foraminifera, Southern England, *J. Foraminifer. Res.*, 31(1), 12–24,
657 doi:10.2113/0310012, 2001.

658 Anschutz, P., Dedieu, K., Desmazes, F. and Chaillou, G.: Speciation, oxidation state, and
659 reactivity of particulate manganese in marine sediments, *Chem. Geol.*, 218(3–4), 265–279,
660 doi:10.1016/j.chemgeo.2005.01.008, 2005.

661 Anschutz, P., Zhong, S., Sundby, B., Mucci, A. and Gobeil, C.: Burial efficiency of
662 phosphorus and the geochemistry of iron in continental margin sediments, *Limnol. Oceanogr.*,
663 43(1), 53–64, 1998.

664 Arndt, S., J orgensen, B. B., LaRowe, D. E., Middelburg, J. J., Pancost, R. D. and Regnier, P.:
665 Quantifying the degradation of organic matter in marine sediments: A review and synthesis,
666 *Earth-Sci. Rev.*, 123, 53–86, doi:10.1016/j.earscirev.2013.02.008, 2013.

667 Barmawidjaja, D. M., Jorissen, F. J., Puskaric, S. and Zwaan, G. J. van der: Microhabitat
668 selection by benthic Foraminifera in the northern Adriatic Sea, *J. Foraminifer. Res.*, 22(4),
669 297–317, doi:10.2113/gsjfr.22.4.297, 1992.

670 Bennett, W. W., Welsh, D. T., Serriere, A., Panther, J. G. and Teasdale, P. R.: A colorimetric
671 DET technique for the high-resolution measurement of two-dimensional alkalinity
672 distributions in sediment porewaters, *Chemosphere*, 119, 547–552,
673 doi:10.1016/j.chemosphere.2014.07.042, 2015.

- 674 Benyoucef, I.: Télédétection visible proche-infrarouge de la distribution spatio-temporelle du
675 microphytobenthos estuarien, Ph.D. thesis, Université de Nantes, 4 August., 2014.
- 676 Benyoucef, I., Blandin, E., Lerouxel, A., Jesus, B., Rosa, P., Méléder, V., Launeau, P. and
677 Barillé, L.: Microphytobenthos interannual variations in a north-European estuary (Loire
678 estuary, France) detected by visible-infrared multispectral remote sensing, *Estuar. Coast.*
679 *Shelf Sci.*, 136, 43–52, doi:10.1016/j.ecss.2013.11.007, 2014.
- 680 Berg, P., Risgaard-Petersen, N. and Rysgaard, S.: Interpretation of measured concentration
681 profiles in sediment pore water, *Limnol. Oceanogr.*, 43(7), 1500–1510,
682 doi:10.4319/lo.1998.43.7.1500, 1998.
- 683 Berkeley, A., Perry, C. T., Smithers, S. G., Horton, B. P. and Taylor, K. G.: A review of the
684 ecological and taphonomic controls on foraminiferal assemblage development in intertidal
685 environments, *Earth-Sci. Rev.*, 83(3–4), 205–230, doi:10.1016/j.earscirev.2007.04.003, 2007.
- 686 Berner, R. A.: Sedimentary pyrite formation, *Am. J. Sci.*, 268(1), 1–23,
687 doi:10.2475/ajs.268.1.1, 1970.
- 688 Bernhard, J. M. and Alve, E.: Survival, ATP pool, and ultrastructural characterization of
689 benthic foraminifera from Drammensfjord (Norway): response to anoxia, *Mar.*
690 *Micropaleontol.*, 28(1), 5–17, doi:10.1016/0377-8398(95)00036-4, 1996.
- 691 Bernhard, J. M., Ostermann, D. R., Williams, D. S. and Blanks, J. K.: Comparison of two
692 methods to identify live benthic foraminifera: A test between Rose Bengal and CellTracker
693 Green with implications for stable isotope paleoreconstructions, *Paleoceanography*, 21(4),
694 PA4210, doi:10.1029/2006PA001290, 2006.
- 695 Bernhard, J. M. and Sen Gupta, B. K. S.: Foraminifera of oxygen-depleted environments, in
696 *Modern Foraminifera*, pp. 201–216, Springer Netherlands. [online] Available from:
697 http://link.springer.com/chapter/10.1007/0-306-48104-9_12 (Accessed 27 November 2014),
698 2003.
- 699 Bivand, R., Pebesma, E. and Gomez-Rubio, V.: *Applied Spatial Data Analysis with R*,
700 Springer New York, New York, NY. [online] Available from:
701 <http://link.springer.com/10.1007/978-0-387-78171-6> (Accessed 16 August 2014), 2008.
- 702 Blanchard, G.: Overlapping microscale dispersion patterns of meiofauna and
703 microphytobenthos, *Mar. Ecol. Prog. Ser.*, 68, 101–111, doi:10.3354/meps068101, 1990.
- 704 Borcard, D., Gillet, F. and Legendre, P.: *Numerical Ecology with R*, Springer New York,
705 New York, NY. [online] Available from: <http://link.springer.com/10.1007/978-1-4419-7976-6>
706 (Accessed 16 August 2014), 2011.
- 707 Bouchet, V. M. P., Sauriau, P.-G., Debenay, J.-P., Mermillod-Blondin, F., Schmidt, S.,
708 Amiard, J.-C. and Dupas, B.: Influence of the mode of macrofauna-mediated bioturbation on
709 the vertical distribution of living benthic foraminifera: First insight from axial
710 tomodesitometry, *J. Exp. Mar. Biol. Ecol.*, 371(1), 20–33, doi:10.1016/j.jembe.2008.12.012,
711 2009.
- 712 Boudreau, B. P.: A method-of-lines code for carbon and nutrient diagenesis in aquatic
713 sediments, *Comput. Geosci.*, 22(5), 479–496, 1996.

- 714 Burdige, D. J.: 5.09 - Estuarine and Coastal Sediments – Coupled Biogeochemical Cycling, in
715 Treatise on Estuarine and Coastal Science, edited by E. Wolanski and D. McLusky, pp. 279–
716 316, Academic Press, Waltham. [online] Available from:
717 <http://www.sciencedirect.com/science/article/pii/B9780123747112005118> (Accessed 26
718 March 2015), 2011.
- 719 Buzas: On the spatial distribution of foraminifera., *Contrib. Cushman Found. Foraminifer.*
720 *Res.*, 19, 1–11, 1968.
- 721 Buzas, M. A.: Spatial Homogeneity: Statistical Analyses of Unispecies and Multispecies
722 Populations of Foraminifera, *Ecology*, 51(5), 874, doi:10.2307/1933980, 1970.
- 723 Buzas, M. A., Hayek, L.-A. C., Jett, J. A. and Reed, S. A.: Pulsating Patches: History and
724 Analyses of Spatial, Seasonal, and Yearly Distribution of Living Benthic Foraminifera,
725 *Smithson. Contrib. Paleobiology*, (97), 2015.
- 726 Buzas, M. A., Hayek, L.-A. C., Reed, S. A. and Jett, J. A.: Foraminiferal Densities Over Five
727 Years in the Indian River Lagoon, Florida: A Model of Pulsating Patches, *J. Foraminifer.*
728 *Res.*, 32(1), 68–92, doi:10.2113/0320068, 2002.
- 729 Cesbron, F., Metzger, E., Launeau, P., Deflandre, B., Delgard, M.-L., Thibault de Chanvalon,
730 A., Geslin, E., Anschutz, P. and Jézéquel, D.: Simultaneous 2D Imaging of Dissolved Iron
731 and Reactive Phosphorus in Sediment Porewaters by Thin-Film and Hyperspectral Methods,
732 *Environ. Sci. Technol.*, 48(5), 2816–2826, doi:10.1021/es404724r, 2014.
- 733 Clark, W. C.: Scales of climate impacts, *Clim. Change*, 7(1), 5–27, 1985.
- 734 Davison, W. and Zhang, H.: In situ speciation measurements of trace components in natural
735 waters using thin-film gels, *Nature*, 367(6463), 546–548, doi:10.1038/367546a0, 1994.
- 736 Debenay, J.-P., Bicchi, E., Goubert, E. and Armynot du Châtelet, E.: Spatio-temporal
737 distribution of benthic foraminifera in relation to estuarine dynamics (Vie estuary, Vendée, W
738 France), *Estuar. Coast. Shelf Sci.*, 67(1–2), 181–197, doi:10.1016/j.ecss.2005.11.014, 2006.
- 739 Debenay, J.-P. and Guillou, J.-J.: Ecological transitions indicated by foraminiferal
740 assemblages in paralic environments, *Estuaries*, 25(6), 1107–1120, doi:10.1007/BF02692208,
741 2002.
- 742 Douglas, R. G.: Paleogeology of continental margin basins: a modern case history from the
743 borderland of southern California, 1981.
- 744 Eckman, J. E. and Thistle, D.: Small-scale spatial pattern in meiobenthos in the San Diego
745 Trough, *Deep Sea Res. Part Oceanogr. Res. Pap.*, 35(9), 1565–1578, doi:10.1016/0198-
746 0149(88)90103-3, 1988.
- 747 Ernst, S., Bours, R., Duijnste, I. and van der Zwaan, B.: Experimental effects of an organic
748 matter pulse and oxygen depletion on a benthic foraminiferal shelf community, *J.*
749 *Foraminifer. Res.*, 35(3), 177–197, 2005.
- 750 Ernst, S. R., Morvan, J., Geslin, E., Le Bihan, A. and Jorissen, F. J.: Benthic foraminiferal
751 response to experimentally induced Erika oil pollution, *Mar. Micropaleontol.*, 61(1-3), 76–93,
752 doi:10.1016/j.marmicro.2006.05.005, 2006.

- 753 Fenchel, T.: Worm burrows and oxic microniches in marine sediments. 1. Spatial and
754 temporal scales, *Mar. Biol.*, 127(2), 289–295, doi:10.1007/BF00942114, 1996.
- 755 Fontanier, C., Jorissen, F. J., Licari, L., Alexandre, A., Anschutz, P. and Carbonel, P.: Live
756 benthic foraminiferal faunas from the Bay of Biscay: faunal density, composition, and
757 microhabitats, *Deep Sea Res. Part Oceanogr. Res. Pap.*, 49(4), 751–785, doi:10.1016/S0967-
758 0637(01)00078-4, 2002.
- 759 Fortin, M.-J. and Dale, M. R. T.: *Spatial analysis a guide for ecologists*, Cambridge
760 University Press, Cambridge, N.Y. [online] Available from:
761 <http://public.eblib.com/EBLPublic/PublicView.do?ptiID=228304> (Accessed 16 August 2014),
762 2005.
- 763 François, F., Gerino, M., Stora, G., Durbec, J. and Poggiale, J.: Functional approach to
764 sediment reworking by gallery-forming macrobenthic organisms: modeling and application
765 with the polychaete *Nereis diversicolor*, *Mar. Ecol. Prog. Ser.*, 229, 127–136,
766 doi:10.3354/meps229127, 2002.
- 767 Froelich, P. N., Klinkhammer, G. P., Bender, M. L., Luedtke, N. A., Heath, G. R., Cullen, D.,
768 Dauphin, P., Hammond, D., Hartman, B. and Maynard, V.: Early oxidation of organic matter
769 in pelagic sediments of the eastern equatorial Atlantic: suboxic diagenesis, *Geochim.*
770 *Cosmochim. Acta*, 43(7), 1075–1090, doi:10.1016/0016-7037(79)90095-4, 1979.
- 771 Geslin, E., Barras, C., Langlet, D., Nardelli, M. P., Kim, J.-H., Bonnin, J., Metzger, E. and
772 Jorissen, F. J.: Survival, Reproduction and Calcification of Three Benthic Foraminiferal
773 Species in Response to Experimentally Induced Hypoxia, in *Approaches to Study Living*
774 *Foraminifera*, edited by H. Kitazato and J. M. Bernhard, pp. 163–193, Springer Japan.
775 [online] Available from: http://link.springer.com/chapter/10.1007/978-4-431-54388-6_10
776 (Accessed 20 August 2014), 2014.
- 777 Geslin, E., Heinz, P., Jorissen, F. and Hemleben, C.: Migratory responses of deep-sea benthic
778 foraminifera to variable oxygen conditions: laboratory investigations, *Mar. Micropaleontol.*,
779 53(3–4), 227–243, doi:10.1016/j.marmicro.2004.05.010, 2004.
- 780 Goldstein, S. T., Watkins, G. T. and Kuhn, R. M.: Microhabitats of salt marsh foraminifera:
781 St. Catherines Island, Georgia, USA, *Mar. Micropaleontol.*, 26(1–4), 17–29,
782 doi:10.1016/0377-8398(95)00006-2, 1995.
- 783 Gross, O.: Influence of temperature, oxygen and food availability on the migrational activity
784 of bathyal benthic foraminifera: evidence by microcosm experiments, in *Life at Interfaces and*
785 *Under Extreme Conditions*, edited by G. Liebezeit, S. Dittmann, and I. Kröncke, pp. 123–137,
786 Springer Netherlands. [online] Available from: http://link.springer.com/chapter/10.1007/978-94-011-4148-2_12
787 (Accessed 3 October 2014), 2000.
- 788 Heinz, P. and Geslin, E.: Ecological and Biological Response of Benthic Foraminifera Under
789 Oxygen-Depleted Conditions: Evidence from Laboratory Approaches, in *Anoxia*, edited by A.
790 V. Altenbach, J. M. Bernhard, and J. Seckbach, pp. 287–303, Springer Netherlands. [online]
791 Available from: http://link.springer.com/chapter/10.1007/978-94-007-1896-8_15 (Accessed 7
792 January 2015), 2012.

- 793 Hess, S., Alve, E., Trannum, H. C. and Norling, K.: Benthic foraminiferal responses to water-
794 based drill cuttings and natural sediment burial: Results from a mesocosm experiment, *Mar.*
795 *Micropaleontol.*, 101, 1–9, doi:10.1016/j.marmicro.2013.03.004, 2013.
- 796 Hofmann, A. F., Soetaert, K., Middelburg, J. J. and Meysman, F. J. R.: AquaEnv : An Aqua
797 tic Acid–Base Modelling Environment in R, *Aquat. Geochem.*, 16(4), 507–546,
798 doi:10.1007/s10498-009-9084-1, 2010.
- 799 Hohenegger, J., Piller, W. and Baal, C.: Reasons for spatial microdistributions of foraminifers
800 in an intertidal pool (northern Adriatic Sea), *Mar. Ecol.*, 10(1), 43–78, 1989.
- 801 Hohenegger, J., Piller, W. E. and Baal, C.: Horizontal and vertical spatial microdistribution of
802 foraminifers in the shallow subtidal Gulf of Trieste, northern Adriatic Sea, *J. Foraminifer.*
803 *Res.*, 23(2), 79–101, doi:10.2113/gsjfr.23.2.79, 1993.
- 804 Hyacinthe, C., Anschutz, P., Carbonel, P., Jouanneau, J.-M. and Jorissen, F. J.: Early
805 diagenetic processes in the muddy sediments of the Bay of Biscay, *Mar. Geol.*, 177(1–2),
806 111–128, doi:10.1016/S0025-3227(01)00127-X, 2001.
- 807 Hyacinthe, C., Bonneville, S. and Van Cappellen, P.: Reactive iron(III) in sediments:
808 Chemical versus microbial extractions, *Geochim. Cosmochim. Acta*, 70(16), 4166–4180,
809 doi:10.1016/j.gca.2006.05.018, 2006.
- 810 Hyacinthe, C. and Van Cappellen, P.: An authigenic iron phosphate phase in estuarine
811 sediments: composition, formation and chemical reactivity, *Mar. Chem.*, 91(1–4), 227–251,
812 doi:10.1016/j.marchem.2004.04.006, 2004.
- 813 Jézéquel, D., Brayner, R., Metzger, E., Viollier, E., Prévot, F. and Fiévet, F.: Two-
814 dimensional determination of dissolved iron and sulphur species in marine sediment pore-
815 waters by thin-film based imaging. Thau lagoon (France), *Estuar. Coast. Shelf Sci.*, 72(3),
816 420–431, doi:10.1016/j.ecss.2006.11.031, 2007.
- 817 Jorissen, F. J.: Benthic foraminifera from the Adriatic Sea: principles of phenotypic variation,
818 *Utrecht Micropaleontol. Bull.*, 37, 1988.
- 819 Jorissen, F. J.: Benthic foraminiferal microhabitats below the sediment-water interface, in
820 *Modern Foraminifera*, pp. 161–179, Springer Netherlands. [online] Available from:
821 http://link.springer.com/chapter/10.1007/0-306-48104-9_10 (Accessed 20 August 2014),
822 2003.
- 823 Jorissen, F. J., Barmawidjaja, D. M., Puskaric, S. and van der Zwaan, G. J.: Vertical
824 distribution of benthic foraminifera in the northern Adriatic Sea: The relation with the organic
825 flux, *Mar. Micropaleontol.*, 19(1–2), 131–146, doi:10.1016/0377-8398(92)90025-F, 1992.
- 826 Jorissen, F. J., de Stigter, H. C. and Widmark, J. G. V.: A conceptual model explaining
827 benthic foraminiferal microhabitats, *Mar. Micropaleontol.*, 26(1–4), 3–15, doi:10.1016/0377-
828 8398(95)00047-X, 1995.
- 829 Jorissen, F. J., Wittling, I., Peypouquet, J. P., Rabouille, C. and Relexans, J. C.: Live benthic
830 foraminiferal faunas off Cape Blanc, NW-Africa: Community structure and microhabitats,
831 *Deep Sea Res. Part Oceanogr. Res. Pap.*, 45(12), 2157–2188, doi:10.1016/S0967-
832 0637(98)00056-9, 1998.

- 833 Koller, H., Dworschak, P. C. and Abed-Navandi, D.: Burrows of *Pestarella tyrrhena*
834 (Decapoda: Thalassinidea): hot spots for Nematoda, Foraminifera and bacterial densities, J.
835 Mar. Biol. Assoc. U. K., 86(5), 1113–1122, 2006.
- 836 Kostka, J. E. and Luther III, G. W.: Seasonal cycling of Fe in saltmarsh sediments,
837 Biogeochemistry, 29(2), 159–181, 1995.
- 838 Kristensen, E., PenhaLopes, G., Delefosse, M., Valdemarsen, T., Quintana, C. O. and Banta,
839 G. T.: REVIEW What is bioturbation? The need for a precise definition for fauna in aquatic
840 sciences, Mar. Ecol. Prog. Ser., 446, 285–302, doi:10.3354/meps09506, 2012.
- 841 Krom, M. D., Davison, P., Zhang, H. and Davison, W.: High-resolution pore-water sampling
842 with a gel sampler, Limnol. Oceanogr., 39(8), 1967–1972, 1994.
- 843 Langezaal, A. M., Ernst, S. R., Haese, R. R., van Bergen, P. F. and van der Zwaan, G. J.:
844 Disturbance of intertidal sediments: the response of bacteria and foraminifera, Estuar. Coast.
845 Shelf Sci., 58(2), 249–264, doi:10.1016/S0272-7714(03)00078-7, 2003.
- 846 Langezaal, A. M., Jorissen, F. J., Braun, B., Chaillou, G., Fontanier, C., Anschutz, P. and van
847 der Zwaan, G. J.: The influence of seasonal processes on geochemical profiles and
848 foraminiferal assemblages on the outer shelf of the Bay of Biscay, Cont. Shelf Res., 26(15),
849 1730–1755, doi:10.1016/j.csr.2006.05.005, 2006.
- 850 Langlet, D., Geslin, E., Baal, C., Metzger, E., Lejzerowicz, F., Riedel, B., Zuschin, M.,
851 Pawlowski, J., Stachowitsch, M. and Jorissen, F. J.: Foraminiferal survival after long-term in
852 situ experimentally induced anoxia, Biogeosciences, 10(11), 7463–7480, doi:10.5194/bg-10-
853 7463-2013, 2013.
- 854 Le Floch, J.-F.: Propagation de la marée dynamique dans l'estuaire de la Seine et en Seine
855 maritime., Thèse d'Etat, Paris., 1961.
- 856 Legendre and Fortin: Spatial pattern and ecological analysis, Vegetation, 80, 107–138, 1989.
- 857 Legendre, P. and Fortin, M.-J.: Comparison of the Mantel test and alternative approaches for
858 detecting complex multivariate relationships in the spatial analysis of genetic data, Mol. Ecol.
859 Resour., 10(5), 831–844, doi:10.1111/j.1755-0998.2010.02866.x, 2010.
- 860 Leutenegger, S. and Hansen, H. J.: Ultrastructural and radiotracer studies of pore function in
861 foraminifera, Mar. Biol., 54(1), 11–16, doi:10.1007/BF00387046, 1979.
- 862 Loubere, P., Jacobsen, B., Klitgaard Kristensen, D., Husum, K., Jernas, P. and Richaud, M.:
863 The structure of benthic environments and the paleochemical record of foraminifera, Deep
864 Sea Res. Part Oceanogr. Res. Pap., 58(5), 535–545, doi:10.1016/j.dsr.2011.02.011, 2011.
- 865 Lovley, D. R.: Dissimilatory Fe(III) and Mn(IV) reduction., Microbiol. Rev., 55(2), 259–287,
866 1991.
- 867 Lynts, G. W.: Relationship of Sediment-size Distribution to Ecologic Factors in Buttonwood
868 Sound, Florida Bay, J. Sediment. Res., 36(1) [online] Available from:
869 <http://archives.datapages.com/data/sepm/journals/v33-37/data/036/036001/0066.htm>
870 (Accessed 27 November 2014), 1966.

- 871 Martiny, J. B. H., Bohannon, B. J. M., Brown, J. H., Colwell, R. K., Fuhrman, J. A., Green, J.
872 L., Horner-Devine, M. C., Kane, M., Krumins, J. A., Kuske, C. R., Morin, P. J., Naeem, S.,
873 Øvreås, L., Reysenbach, A.-L., Smith, V. H. and Staley, J. T.: Microbial biogeography:
874 putting microorganisms on the map, *Nat. Rev. Microbiol.*, 4(2), 102–112,
875 doi:10.1038/nrmicro1341, 2006.
- 876 Meyers, M. B., Fossing, H. and Powell, E. N.: Microdistribution of interstitial meiofauna,
877 oxygen and sulphide gradients, and the tubes of macro-infauna, *Mar. Ecol.-Prog. Ser.*, 35,
878 223–241, doi:10.3354/meps035223, 1987.
- 879 Meysman, F. J., Boudreau, B. P. and Middelburg, J. J.: When and why does bioturbation lead
880 to diffusive mixing?, *J. Mar. Res.*, 68(6), 881–920, 2010a.
- 881 Meysman, F. J. R., Boudreau, B. P. and Middelburg, J. J.: Relations between local, nonlocal,
882 discrete and continuous models of bioturbation, *J. Mar. Res.*, 61(3), 391–410,
883 doi:10.1357/002224003322201241, 2003.
- 884 Meysman, F. J. R., Galaktionov, O. S., Glud, R. N. and Middelburg, J. J.: Oxygen penetration
885 around burrows and roots in aquatic sediments, *J. Mar. Res.*, 68(2), 309–336,
886 doi:10.1357/002224010793721406, 2010b.
- 887 Meysman, F. J. R., Malyuga, V. S., Boudreau, B. P. and Middelburg, J. J.: A generalized
888 stochastic approach to particle dispersal in soils and sediments, *Geochim. Cosmochim. Acta*,
889 72(14), 3460–3478, doi:10.1016/j.gca.2008.04.023, 2008.
- 890 Meysman, F. J. R., Middelburg, J. J. and Heip, C. H. R.: Bioturbation: a fresh look at
891 Darwin's last idea, *Trends Ecol. Evol.*, 21(12), 688–695, doi:10.1016/j.tree.2006.08.002,
892 2006.
- 893 Millero, F. J.: The thermodynamics of the carbonate system in seawater, *Geochim.*
894 *Cosmochim. Acta*, 43(10), 1651–1661, doi:10.1016/0016-7037(79)90184-4, 1979.
- 895 Millero, F. J.: Thermodynamics of the carbon dioxide system in the oceans, *Geochim.*
896 *Cosmochim. Acta*, 59(4), 661–677, doi:10.1016/0016-7037(94)00354-O, 1995.
- 897 Moodley, L.: Southern North Sea seafloor and subsurface distribution of living benthic
898 foraminifera, *Neth. J. Sea Res.*, 27(1), 57–71, doi:10.1016/0077-7579(90)90034-E, 1990.
- 899 Moodley, L. and Hess, C.: Tolerance of Infaunal Benthic Foraminifera for Low and High
900 Oxygen Concentrations, *Biol. Bull.*, 183(1), 94–98, 1992.
- 901 Moodley, L., van der Zwaan, G. J., Rutten, G. M. W., Boom, R. C. E. and Kempers, A. J.:
902 Subsurface activity of benthic foraminifera in relation to porewater oxygen content:
903 laboratory experiments, *Mar. Micropaleontol.*, 34(1–2), 91–106, doi:10.1016/S0377-
904 8398(97)00044-3, 1998.
- 905 Morse, J. W., DiMarco, S. F., Hebert, A. B. and Sell, K. S.: A scaling approach to spatial
906 variability in early diagenetic processes, in *The Interactions between Sediments and Water*,
907 pp. 25–29, Springer. [online] Available from: [http://link.springer.com/chapter/10.1007/978-](http://link.springer.com/chapter/10.1007/978-94-017-3366-3_5)
908 [94-017-3366-3_5](http://link.springer.com/chapter/10.1007/978-94-017-3366-3_5) (Accessed 30 June 2014), 2003.

- 909 Morvan, J., Debenay, J.-P., Jorissen, F., Redois, F., Bénéteau, E., Delplancke, M. and Amato,
910 A.-S.: Patchiness and life cycle of intertidal foraminifera: Implication for environmental and
911 paleoenvironmental interpretation, *Mar. Micropaleontol.*, 61(1-3), 131–154,
912 doi:10.1016/j.marmicro.2006.05.009, 2006.
- 913 Mucci, A.: The solubility of calcite and aragonite in seawater at various salinities,
914 temperatures, and one atmosphere total pressure, *Am. J. Sci.*, 283(7), 780–799,
915 doi:10.2475/ajs.283.7.780, 1983.
- 916 Mucci, A., Sundby, B., Gehlen, M., Arakaki, T., Zhong, S. and Silverberg, N.: The fate of
917 carbon in continental shelf sediments of eastern Canada: a case study, *Deep Sea Res. Part II*
918 *Top. Stud. Oceanogr.*, 47(3–4), 733–760, doi:10.1016/S0967-0645(99)00124-1, 2000.
- 919 Nardelli, M. P., Barras, C., Metzger, E., Mouret, A., Filipsson, H. L., Jorissen, F. and Geslin,
920 E.: Experimental evidence for foraminiferal calcification under anoxia, *Biogeosciences*,
921 11(14), 4029–4038, doi:10.5194/bg-11-4029-2014, 2014.
- 922 Nomaki, H., Chikaraishi, Y., Tsuchiya, M., Toyofuku, T., Ohkouchi, N., Uematsu, K., Tame,
923 A. and Kitazato, H.: Nitrate uptake by foraminifera and use in conjunction with endobionts
924 under anoxic conditions, *Limnol. Oceanogr.*, 59(6), 1879–1888,
925 doi:10.4319/lo.2014.59.6.1879, 2014.
- 926 Paterson, D. M.: Short-term changes in the erodibility of intertidal cohesive sediments related
927 to the migratory behavior of epipelagic diatoms, *Limnol. Oceanogr.*, 34(1), 223–234, 1989.
- 928 Phipps, M. Daniel: Benthic foraminifera of the Portuguese margin: Impact of organic supplies
929 on the density, biodiversity and composition of the faunas, *Université d'Angers*. [online]
930 Available from: <https://tel.archives-ouvertes.fr/tel-00993121/> (Accessed 28 April 2015), 2012.
- 931 Pina-Ochoa, E., Hogslund, S., Geslin, E., Cedhagen, T., Revsbech, N. P., Nielsen, L. P.,
932 Schweizer, M., Jorissen, F., Rysgaard, S. and Risgaard-Petersen, N.: Widespread occurrence
933 of nitrate storage and denitrification among Foraminifera and Gromiida, *Proc. Natl. Acad.*
934 *Sci.*, 107(3), 1148–1153, doi:10.1073/pnas.0908440107, 2010.
- 935 Pishedda, L., Cuny, P., Esteves, J. L., Poggiale, J.-C. and Gilbert, F.: Spatial oxygen
936 heterogeneity in a *Hediste diversicolor* irrigated burrow, *Hydrobiologia*, 680(1), 109–124,
937 doi:10.1007/s10750-011-0907-x, 2012.
- 938 Pucci, F., Geslin, E., Barras, C., Morigi, C., Sabbatini, A., Negri, A. and Jorissen, F. J.:
939 Survival of benthic foraminifera under hypoxic conditions: Results of an experimental study
940 using the CellTracker Green method, *Mar. Pollut. Bull.*, 59(8–12), 336–351,
941 doi:10.1016/j.marpolbul.2009.08.015, 2009.
- 942 Revsbech, N. P., Sørensen, J., Blackburn, T. H. and Lomholt, J. P.: Distribution of oxygen in
943 marine sediments measured with microelectrodes, *Limnol. Oceanogr.*, 25(3), 403–411,
944 doi:10.4319/lo.1980.25.3.0403, 1980.
- 945 Richter, G.: Beobachtungen zur Ökologie einiger Foraminiferen des Jade Gebietes, *Nat.*
946 *Volk*, 91, 163–170, 1961.
- 947 Risgaard-Petersen, N., Langezaal, A. M., Ingvarsdson, S., Schmid, M. C., Jetten, M. S. M., Op
948 den Camp, H. J. M., Derksen, J. W. M., Piña-Ochoa, E., Eriksson, S. P., Peter Nielsen, L.,

- 949 Peter Revsbech, N., Cedhagen, T. and van der Zwaan, G. J.: Evidence for complete
950 denitrification in a benthic foraminifer, *Nature*, 443(7107), 93–96, doi:10.1038/nature05070,
951 2006.
- 952 Robertson, D., Teasdale, P. R. and Welsh, D. T.: A novel gel-based technique for the high
953 resolution, two-dimensional determination of iron (II) and sulphide in sediment, *Limnol*
954 *Ocean. Methods*, 6, 502–512, 2008.
- 955 Robertson, D., Welsh, D. T. and Teasdale, P. R.: Investigating biogenic heterogeneity in
956 coastal sediments with two-dimensional measurements of iron(II) and sulphide, *Environ.*
957 *Chem.*, 6(1), 60–69, 2009.
- 958 Round, F.: The ecology of benthic algae, in *Algae and man*, pp. 138–184, Springer., 1964.
- 959 Saffert, H. and Thomas, E.: Living foraminifera and total populations in salt marsh peat cores:
960 Kelsey Marsh (Clinton, CT) and the Great Marshes (Barnstable, MA), *Mar. Micropaleontol.*,
961 33(3–4), 175–202, doi:10.1016/S0377-8398(97)00035-2, 1998.
- 962 Santner, J., Larsen, M., Kreuzeder, A. and Glud, R. N.: Two decades of chemical imaging of
963 solutes in sediments and soils – a review, *Anal. Chim. Acta*, doi:10.1016/j.aca.2015.02.006,
964 2015.
- 965 de Stigter, H. C., van der Zwaan, G. J. and Langone, L.: Differential rates of benthic
966 foraminiferal test production in surface and subsurface sediment habitats in the southern
967 Adriatic Sea, *Palaeogeogr. Palaeoclimatol. Palaeoecol.*, 149(1–4), 67–88, doi:10.1016/S0031-
968 0182(98)00193-X, 1999.
- 969 Stockdale, A., Davison, W. and Zhang, H.: Micro-scale biogeochemical heterogeneity in
970 sediments: A review of available technology and observed evidence, *Earth-Sci. Rev.*, 92(1–2),
971 81–97, doi:10.1016/j.earscirev.2008.11.003, 2009.
- 972 Stockdale, A., Davison, W. and Zhang, H.: Formation of iron sulphide at faecal pellets and
973 other microniches within suboxic surface sediment, *Geochim. Cosmochim. Acta*, 74(9),
974 2665–2676, doi:10.1016/j.gca.2010.02.005, 2010.
- 975 Thibault de Chanvalon, A., Metzger, E., Mouret, A., Geslin, E., Knoery, J. and Meysman, F.
976 J. R.: Iron release from intertidal mudflat: 2D modelling at submillimetre scale., *Mar. Chem.*,
977 in prep.
- 978 Thomsen, L. and Altenbach, A. V.: Vertical and areal distribution of foraminiferal abundance
979 and biomass in microhabitats around inhabited tubes of marine echinurids, *Mar.*
980 *Micropaleontol.*, 20(3–4), 303–309, doi:10.1016/0377-8398(93)90039-Z, 1993.
- 981 Travis, J. L. and Rabalais, N. N.: The motility of Foraminifera, in *Biology of the*
982 *Foraminifera*, in *Biology of the Foraminifera*, pp. 91–155, J.J. Lee O.R. Anderson, London.,
983 1991.
- 984 Vader, W. J. M.: A preliminary investigation into the reactions of the infauna of the tidal flats
985 to tidal fluctuations in water level, *Neth. J. Sea Res.*, 2(2), 189–222, doi:10.1016/0077-
986 7579(64)90009-2, 1964.

- 987 Van der Zwaan, G. J., Duijnste, I. A. P., den Dulk, M., Ernst, S. R., Jannink, N. T. and
988 Kouwenhoven, T. J.: Benthic foraminifers: proxies or problems?: A review of paleocological
989 concepts, *Earth-Sci. Rev.*, 46(1–4), 213–236, doi:10.1016/S0012-8252(99)00011-2, 1999.
- 990 Van der Zwaan, G. J. V. D. and Jorissen, F. J.: Biofacial patterns in river-induced shelf
991 anoxia, *Geol. Soc. Lond. Spec. Publ.*, 58(1), 65–82, doi:10.1144/GSL.SP.1991.058.01.05,
992 1991.
- 993 Wang, F., Tessier, A. and Hare, L.: Oxygen measurements in the burrows of freshwater
994 insects, *Freshw. Biol.*, 46(3), 317–327, 2001.
- 995 Wenzhofer, F. and Glud, R. N.: Small-scale spatial and temporal variability in coastal benthic
996 O₂ dynamics: Effects of fauna activity, *Limnol. Oceanogr.*, 49, 1471–1481, 2004.
- 997 Wheatcroft, R. A., Jumars, P. A., Smith, C. R. and Nowell, A. R. M.: A mechanistic view of
998 the particulate biodiffusion coefficient: step lengths, rest periods and transport directions, *J.*
999 *Mar. Res.*, 48(1), 177–207, 1990.
- 1000 Wu, J., Jelinski, D. E., Luck, M. and Tueller, P. T.: Multiscale Analysis of Landscape
1001 Heterogeneity: Scale Variance and Pattern Metres, *Geogr. Inf. Sci.*, 6(1), 6–19,
1002 doi:10.1080/10824000009480529, 2000.
- 1003 Wu, J. and Li, H.: Concepts of scale and scaling, in *Scaling and uncertainty analysis in*
1004 *ecology*, pp. 3–15, Springer. [online] Available from:
1005 http://link.springer.com/content/pdf/10.1007/1-4020-4663-4_1.pdf (Accessed 22 September
1006 2015), 2006.
- 1007 Zhu, Q. and Aller, R. C.: A rapid response, planar fluorosensor for measuring two-
1008 dimensional pCO₂ distributions and dynamics in marine sediments, *Limnol. Oceanogr.*
1009 *Methods*, 8, 326–336, doi:10.4319/lom.2010.8.326, 2010.
- 1010 Zhu, Q. and Aller, R. C.: Two-dimensional dissolved ferrous iron distributions in marine
1011 sediments as revealed by a novel planar optical sensor, *Mar. Chem.*, 136-137, 14–23,
1012 doi:10.1016/j.marchem.2012.04.002, 2012.
- 1013 Zhu, Q., Aller, R. C. and Fan, Y.: Two-dimensional pH distributions and dynamics in
1014 bioturbated marine sediments, *Geochim. Cosmochim. Acta*, 70(19), 4933–4949,
1015 doi:10.1016/j.gca.2006.07.033, 2006.
- 1016 Zorn, M. E., Lalonde, S. V., Gingras, M. K., Pemberton, S. G. and Konhauser, K. O.:
1017 Microscale oxygen distribution in various invertebrate burrow walls, *Geobiology*, 4(2), 137–
1018 145, doi:10.1111/j.1472-4669.2006.00074.x, 2006.
- 1019
- 1020

1021
1022
1023
1024
1025
1026
1027
1028
1029

1030 **6 Supplementary materials**

1031 **S1 Solid geochemistry**

1032

1033 The two cores were used to constrain geochemistry. They were stored at *in situ* temperature
1034 until processing, and were processed in a field laboratory. The first core was dedicated to
1035 solid phase geochemistry and microelectrode profiling (see section 2.2.3). The solid phase
1036 was characterized by total organic carbon, reactive iron, manganese and phosphorus. After
1037 profiling, the core was sub-sampled using a tube of 3 cm diameter and sliced every 2 mm
1038 until 2 cm and every 5 mm until 5 cm depth (Fig 2 A). After slicing, samples were
1039 immediately frozen with carbonic ice. Within a week, samples were freeze-dried, the weight
1040 difference before and after freeze-drying served to calculate porosity. Next, samples were
1041 manually ground using an agate mortar and separated into two aliquots for chemical analyses.

1042

1043 The first aliquot of freeze-dried sediment (between 50 and 150 mg) was incubated in 10 mL
1044 of a solution of ascorbic acid (buffered at pH 8) during 24 hours to extract the reactive solid
1045 phase. This technique is commonly used (Anschutz et al., 1998; Hyacinthe et al., 2001;
1046 Hyacinthe and Van Cappellen, 2004; Kostka and Luther III, 1995) and allows to extract both
1047 amorphous Fe(III) oxyhydroxides (Kostka and Luther III, 1994) supposedly close to those
1048 reduced by microorganisms (Hyacinthe et al., 2006) as well as Mn(III) and Mn(IV) oxides
1049 (Anschutz et al., 2005). After extraction, samples were centrifuged (15 min at 3000 rpm) and
1050 the supernatant was diluted in Ultrapure© HCl (1% weight). Next, samples were analyzed on
1051 ICP-AES (Thermo Scientific iCAP 6300 Radial), uncertainty is 1, 8 and 4% for respectively
1052 iron, phosphorus and manganese (twice the relative standard deviation of ICP-AES
1053 triplicates). The second aliquot, between 1.5 and 3 mg, was used for organic carbon analysis.
1054 It was performed on EA1110 CHN/S/O (Thermo Fisher) after 1h-extraction in a HCl
1055 saturated atmosphere. Each chromatograph was inspected visually. Accuracy was verified
1056 with standards (MS-61 and B2150) and uncertainty, calculated from standard deviation for ten
1057 replicates from standard MS-61, was 4.5%.

1058

1059 **S2 1D Pore water analysis**

1060

1061 Oxygen, dissolved iron, manganese and phosphorus were analyzed. The core dedicated to
1062 oxygen profiling and solid phase remained emerged in the *in situ* temperature tank. The

1063 sediment water interface was roughly visually estimated during profiling. During data
1064 treatment, the interface was repositioned according to the break visible in the O₂ profile after
1065 the start of the concentration decrease. 18 oxygen profiles (each time two profiles were
1066 measured simultaneously) were realized using Clark's type electrodes (50µm tip diameter)
1067 mounted on an automated micromanipulator (Unisense©, Denmark) within the first 5 mm at a
1068 100 µm vertical resolution. Profiling was done within 1 hour after sampling.

1069

1070 Diffusive Equilibrium in Thin film in one dimension probes (DET 1D, adapted from Davison
1071 and Zhang, 1994; Krom et al., 1994) were used for dissolved iron, manganese and
1072 phosphorus. Two probes were prepared from DGT-Research© supports, less than one week
1073 before deployment. Each support corresponds to 75 cells of 22 µL and has a vertical
1074 resolution of 2 mm. They were cleaned during 1 week using 10 % Suprapur Merck nitric acid
1075 and rinsed three time with milli-Q water (Millipore©). A solution (1.5% w/w) of agarose in
1076 Milli-Q water was poured into the probe, the excess gel was removed with a Teflon-coated
1077 razor blade and then covered with a PVDF hydrophilic membrane (0.2 µm size pore,
1078 Millipore©) (Metzger et al., 2007, 2014). Each probe was conserved in a wet clean plastic bag
1079 and finally bubbled with N₂ during 6h before deployment in the third core. After one night
1080 incubation in the core at *in situ* temperature, probes were retrieved and DET gel pieces were
1081 sampled using a small plastic tip and eluted in 5mL of a 0.01 mol L⁻¹ suprapur© Merck nitric
1082 acid solution (dilution factor of the pore water of about 200). Iron, manganese and phosphorus
1083 were then analyzed by ICP-AES (Thermo Scientific iCAP 6300 Radial). Sodium was
1084 supposed constant through the sediment column, and used as internal standard. Incertitude is
1085 less than 10% for dissolved iron and manganese and 30% for phosphorus.

1086

1087 **S3 2D pore water analysis**

1088

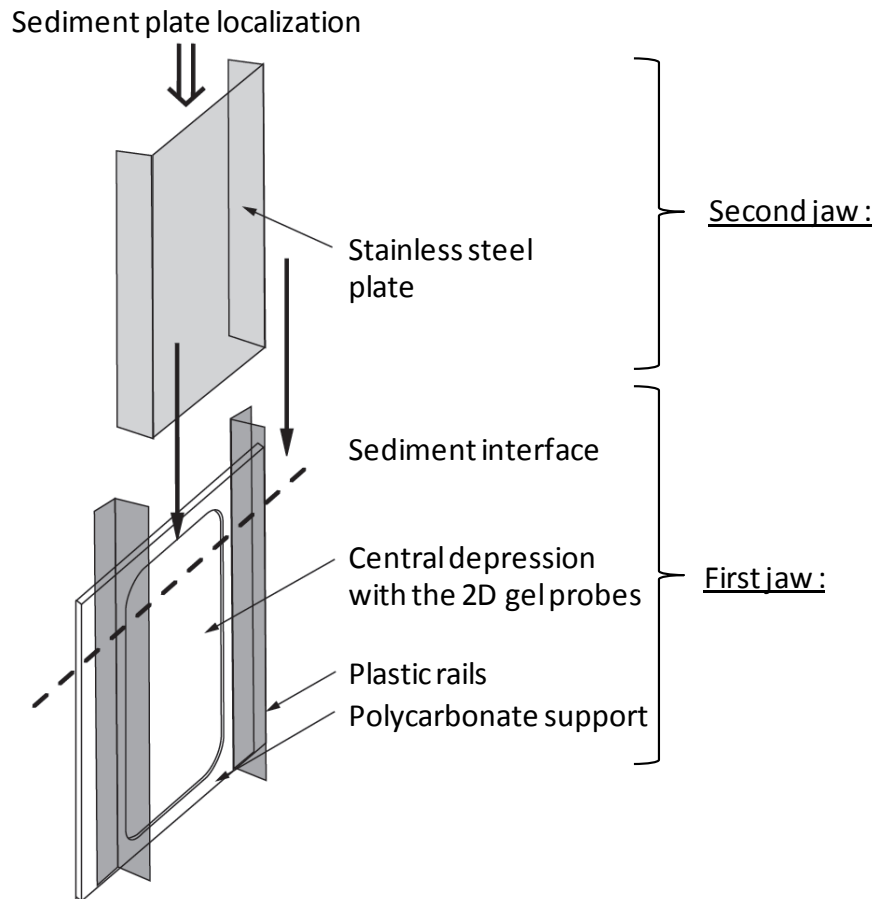
1089 The DET 2D probe was analyzed in order to obtain the concentrations of dissolved iron,
1090 dissolved reactive phosphate (DRP) and the qualitative distribution of H₂S (Cesbron et al.,
1091 2014). The 2D DET probe was unfrozen during 10 minutes at ambient temperature; next, the
1092 plastic-coated aluminum plate was taken out and the polyacrylamide thin-film was taken off.
1093 The PVC adhesive film was scanned with a common commercial flatbed scanner (Canon
1094 Canoscan LiDE 600F) and analyzed in blue intensity (from RGB decomposition) with
1095 ImageJ© software. The unfrozen gel is laid on a white board and recovered by a reactive gel.

1096 The reactive gel was a 0.46mm thick polyacrylamide gel incubated during 1 hour in a reactive
1097 solution containing ascorbic acid $3 \cdot 10^{-2}$ M, sulfuric acid $5.58 \cdot 10^{-1}$ M, potassium antimony(III)
1098 tartrate hydrate $3.2 \cdot 10^{-4}$ M, ammonium molybdate tetrahydrate $1.86 \cdot 10^{-2}$ M and ferrozine 1.22
1099 10^{-2} M, final concentrations. This is an improvement compared to Cesbron et al. (2014) as
1100 only one reactive gel is made, instead of two, reducing handling time considerably.

1101
1102 Twenty five minutes after contact, a picture (reflectance analysis) of superposed gels was
1103 taken with a hyperspectral camera (HySpex VNIR 1600) and analyzed with the software
1104 ENVI (Environment for Visualizing Image, RSI) to obtain DRP and dissolved iron
1105 concentrations. The resolution (length of pixels) was $211 \cdot 216 \mu\text{m}^2$. The HySpex VNIR 1600
1106 camera is sensitive to 160 channels (spectral resolution of 4.5 nm), which is much more
1107 precise than the three channels of 100 nm resolution from standard RGB (Red, Green, Blue)
1108 images. Standards, made following (Cesbron et al., 2014) gave one end-member spectrum for
1109 each measured species (mean of 2470 ± 5 pixels) and a third end-member spectrum for the
1110 background (Fig 4). Next, after logarithmic transformation of reflectance, linear combination
1111 between these three end-members applied on each pixel (of both standard and probe gels),
1112 gave the proportion of each one expressed on that pixel. For the two chemical species, this
1113 proportion was multiplied by the respective known concentration of end-members (here 18.58
1114 μM for DRP and $253.56 \mu\text{M}$ for dissolved iron). Next, a calibration with the standard is made
1115 (six points for each species: from 3.52 to $59.31 \mu\text{M}$ for DRP and from 16.46 to $253.56 \mu\text{M}$ for
1116 iron). The exactness of the method is verified by 1) comparison between measured+calculated
1117 and real concentrations of standards (mean difference of 4,4% for iron and 7,3% for DRP), 2)
1118 the expression of background end-members from linear combination (here 0.95 ± 0.06
1119 compared to the theoretical value of 1.00) and 3) the error from linear combination, here of
1120 $3.4 \pm 0.5\%$. The estimated complete incertitude is then 9,8% for iron and 11,2% for DRP.

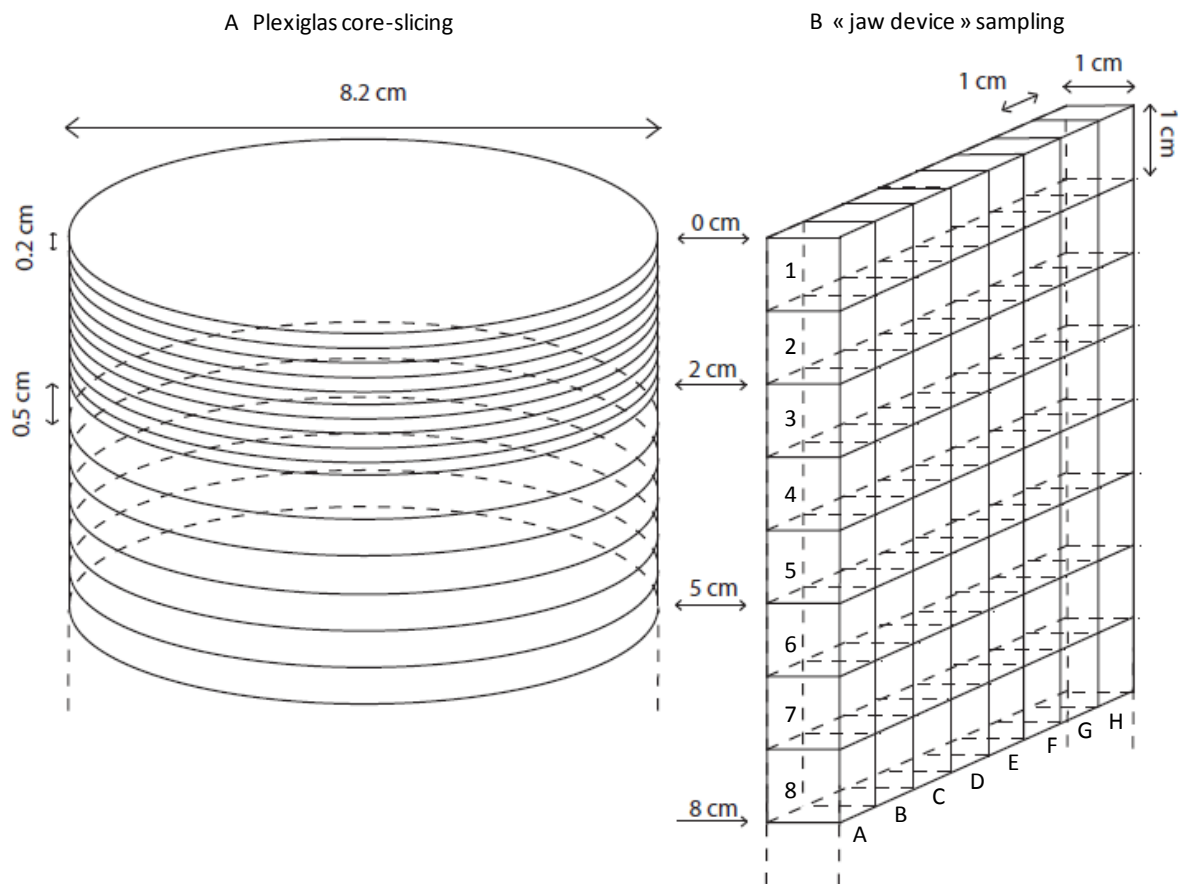
1121
1122 To compare the geochemical species distribution (at submillimeter resolution) with
1123 foraminiferal density (at centimeter resolution), a handmade R code was written allowing the
1124 decrease of chemical resolution from 0.2 mm down to 1 cm. As 1 centimeter is equal to
1125 $46.3 \cdot 47.4$ pixels, the code takes for each centimeter the average concentration of $46 \cdot 47 = 2162$
1126 pixels. Thus $0.3 \cdot 0.4$ pixels are lost for each centimeter square which correspond to 1.27% of
1127 the surface *i.e.* 2.3 cm^2 for the entire gel. This loss is attributed to each side, and then
1128 neglected.

1129



1130
 1131
 1132
 1133
 1134

Figure 1 Schematic view of the "jaw device" for simultaneous sampling of sediment and porewater.



1136

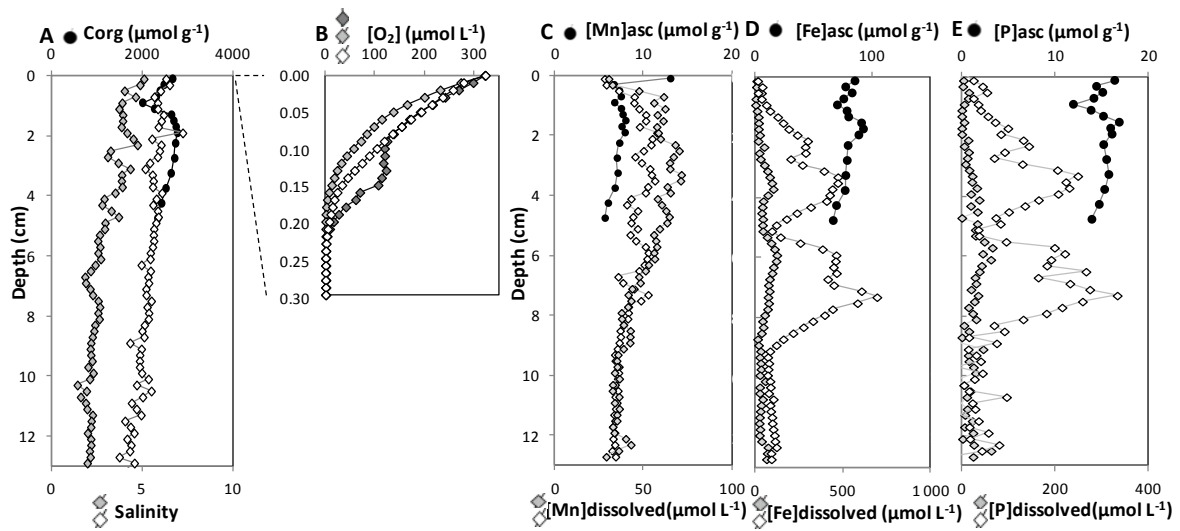
1137

1138

1139

1140

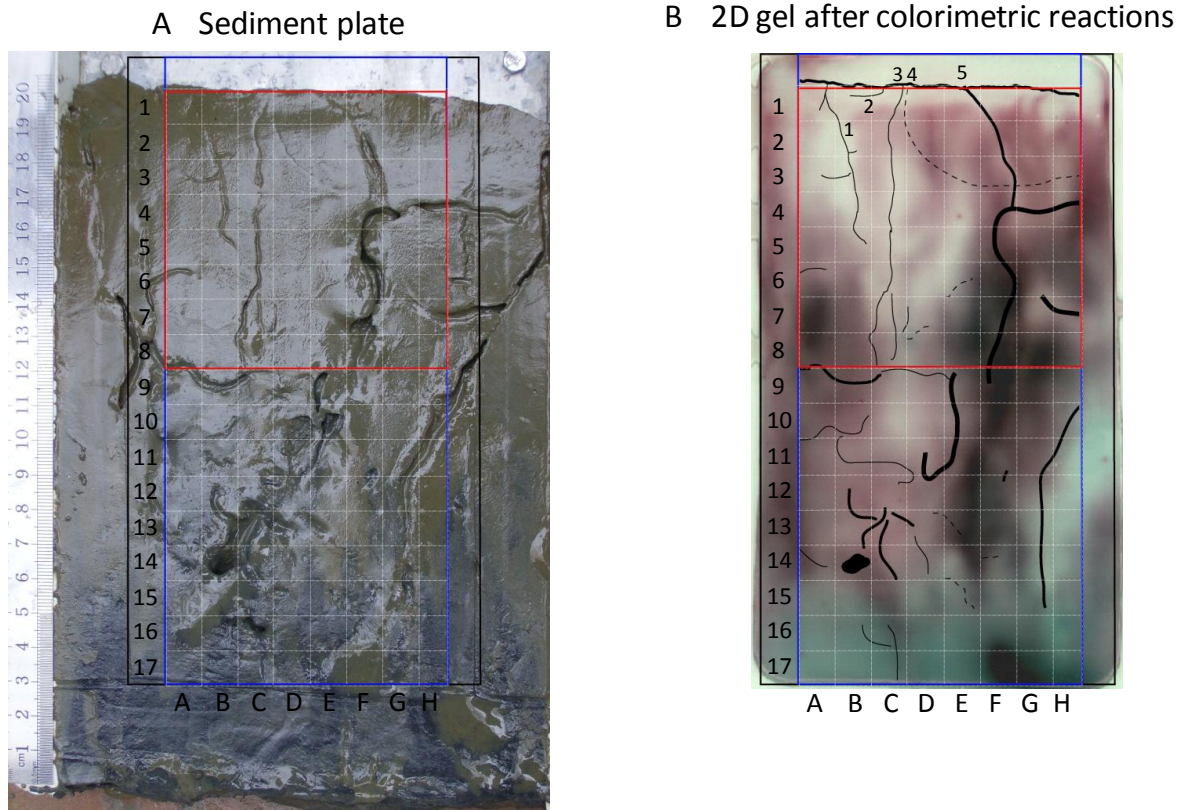
Figure 2. Sediment sampling methodology for living foraminiferal analyses. A: Usual 1D hand coring and layer slicing. B: Sediment plate sampling with the second jaw of the “jaw device” (Fig.1) and representation of the sediment cubic slicing.



1142
 1143
 1144
 1145
 1146
 1147
 1148
 1149

Figure 3: 1D geochemical features A- Vertical profile of total solid organic carbon (filled circles, uncertainty smaller than symbol size) and profiles of salinity (white and grey diamonds). B- Typical profiles of dissolved oxygen, the profile with dark grey diamonds is considered as bioturbated. C, D, E- Vertical profiles of manganese (C), iron (D) and phosphorus (E) in dissolved (white and gray diamonds for DET replicates) and reactive solid phase (ascorbate-leached) from the core (black circles).

1150



1151

1152

1153

1154

1155

1156

1157

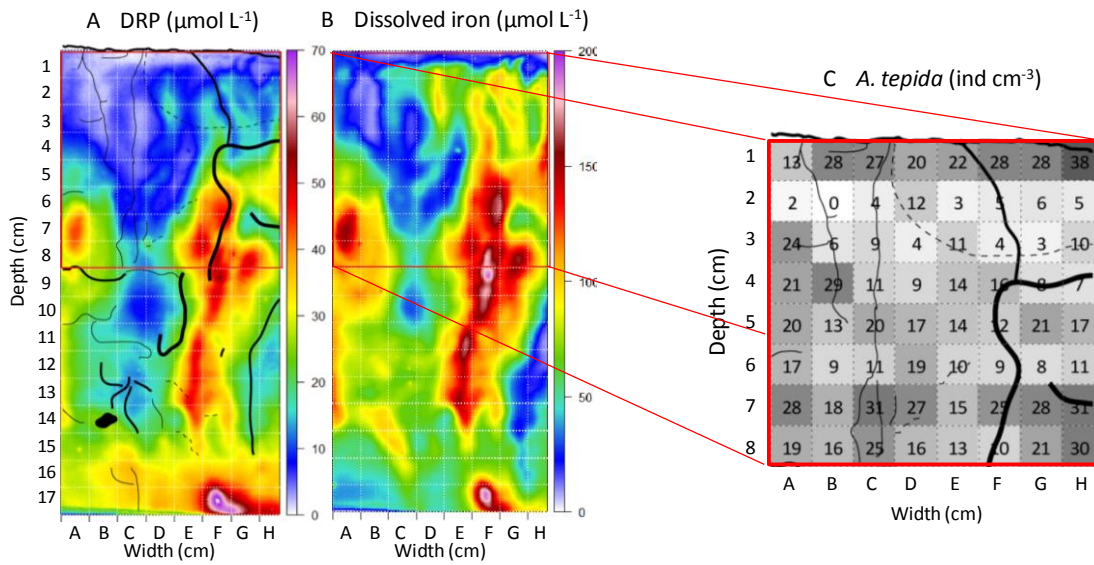
1158

1159

1160

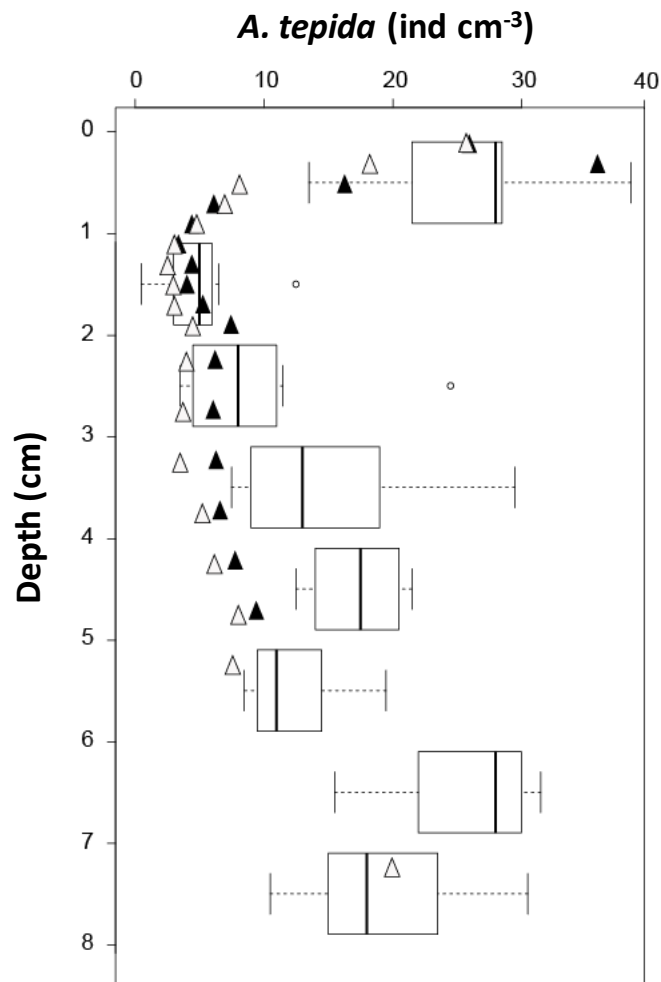
Figure 4: A - Picture of the sediment plate before cube slicing for foraminiferal analysis (sediment water interface at the top). B. Picture of the analyzed gel after colorimetric reactions: dissolved iron shown in dark pink and dissolved phosphorus in turquoise (burrows superimposed). The black rectangle corresponds to the gel limit, the blue rectangle to the limit of available dataset of dissolved iron and phosphorus and the red rectangle to the limit of the available dataset of foraminiferal distribution.

1161

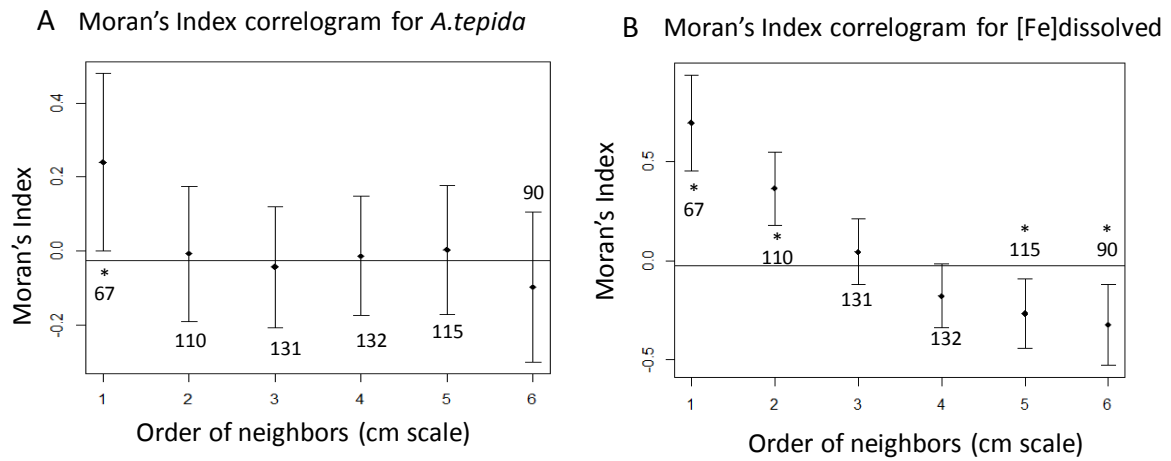


1162
1163
1164
1165
1166
1167

Figure 5: A B - Two dimensional concentrations after numerical analysis of dissolved reactive phosphorus (DRP) and dissolved iron. The distribution of burrows is shown on the DRP plot. Red lines represent the boundary of foraminiferal analysis. C - 2D distribution of *A. tepida* densities from the sediment plate with burrow distribution

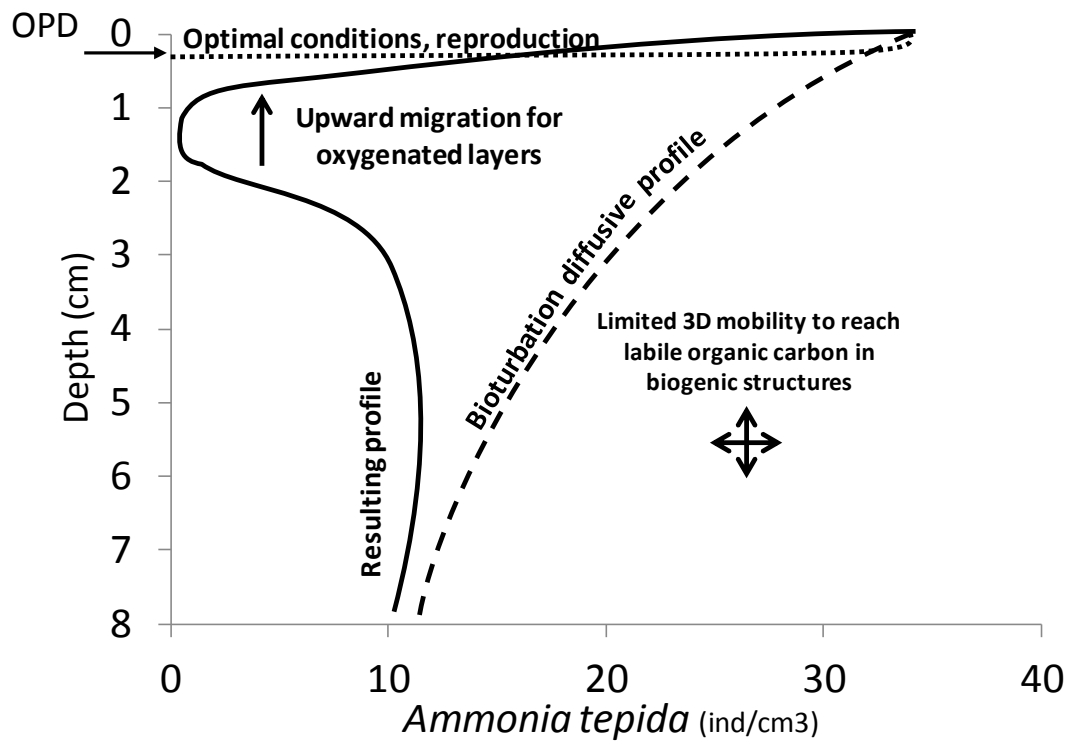


1169
 1170 Figure 6: Vertical comparison of *A. tepida* densities from the 2 cores (full and open triangles)
 1171 and the “jaw device” sampling (each boxplot represents the distribution of one layer; bars are
 1172 first and third quartiles for the boxes length and whiskers are below 1.5 interquartiles; open
 1173 circles are outliers).
 1174
 1175



1177
 1178
 1179
 1180
 1181
 1182
 1183

Figure 7: Moran's Index Correlograms for 3 to 8 cm depth: A- Moran's Index correlogram for *A. tepida* with a 1 cm resolution. B - Moran's Index correlogram for [Fe]dissolved with a 1 cm resolution. * shows significant differences from zero, error bars are twice the standard deviation; the numbers are the number of pairs for each order of neighbours.



1184

1185 Figure 8: Putative mechanisms explaining the *A. tepida* density profile (OPD = Oxygen

1186 Penetration Depth).

1187

1188